AN EXPERIMENTAL STUDY OF THE INELASTIC BEHAVIOR OF SIMPLE BEAMS SUBJECTED TO MOVING LOADS

Thesis for the Degree of M. S.

MICHIGAN STATE UNIVERSITY

Richard Ervin Hills

1965

ABSTRACT

AN EXPERIMENTAL STUDY OF THE INELASTIC BEHAVIOR OF SIMPLE BEAMS SUBJECTED TO MOVING LOADS

by Richard Ervin Hills

An experimental study of the inelastic behavior of simply supported beams under heavy moving unsprung loads is reported. A total of 37 mild steel beams were tested. The beams were 1/4 in. deep by 1 in. wide and 2 ft. long.

The load was in the form of a single-axle unsprung carriage propelled by the energy of a dropping weight to speeds varying from 6 to 16 fps. The weight of the load was varied from 0.9 to 1.3 times the mid-span yield load which is approximately 60 lbs. The mid-span deflections of the beam and the vertical accelerations of the load were recorded in the tests.

It was found that although loads heavier than the yield load could cross the beam, the permanent set increased rapidly as the load exceeded the yield load. Generally, an increase of the load speed caused a rapid increase in the beam response. An analysis of the data indicates that the essential feature of the phenomena lies in an interplay of the curvature, the interacting force, and the bending moment.

AN EXPERIMENTAL STUDY OF THE INELASTIC BEHAVIOR OF SIMPLE BEAMS SUBJECTED TO MOVING LOADS

By

RICHARD ERVIN HILLS

A THESIS

Submitted to
Michigan State University
in partial fulfillment of the requirements
for the degree of

MASTER OF SCIENCE

Department of Civil Engineering

1965

ACKNOWLEDGMENTS

The work reported herein was done as part of an investigation of the inelastic behavior of beams subjected to moving loads conducted in the Department of Civil Engineering of Michigan State University. The project has been sponsored by the National Science Foundation under Grant No. G-12143 administered by the Division of Engineering Research.

This work constitutes the author's thesis, which has been written under the direction of Dr. Robert K. Wen, to whom gratitude is extended for his guidance and instruction. Thanks are expressed to Bethlehem Steel Company and Dr. I. M. Viest, Structural Engineer of that organization, for arranging to supply the steel bars used in this study.

The author wishes to express his appreciation to Mr. Shien Tsun Wang, formerly Special Graduate Research Assistant, for his able assistance in the collection of the data. Special gratitude is extended to the Machine Shop of the College of Engineering for their assistance in fabricating the experimental apparatus.

TABLE OF CONTENTS

LIST OF FIGURES

LIST OF TABLES

I. INTRODUCTION

1.1 Object and Scope.

The problem of moving loads on structures has been the subject of theoretical and experimental investigation by many engineers and scientists. Until recently, the scope of all work has been limited by the assumption that the behavior of the structure-load system is linearly elastic.

More recently, there have been some theoretical studies that have extended the scope and considered the behavior in the inelastic range (1-4). However, except for the work reported in (7), there has been no experimental work reported that considered the inelastic behavior. (Actually, the work described in (7) was subsequent to that reported herein. Because the author was called to military service, the reporting of the present work was delayed until this time.)

Since the end of World War II there has been a trend toward adopting the ultimate strength concept for structural design. It is evident that in order to develop a rational method of bridge design based on that concept, it is of basic importance to understand the inelastic behavior of structures subjected to moving loads. The present work represents an effort in that direction.

The present study is limited to simply supported beams subjected to unsprung loads --- loads that are not supported by springs or suspension systems. It essentially consists of two parts. First, the design and construction of a laboratory set-up for the study, and secondly, the execution of a series of tests

and the analysis of the data.

All beams tested were made of mild steel; each beam is 2 ft. long and has a rectangular cross-section of 1 in. by 1/4 in. The study considered two parameters: the speed of the load (varied from a "crawl" to 16 fps), and the magnitude of the load (varied from 0.9 to 1.3 times the "static yield load" --- the load that, if applied statically at mid-span, would initiate yielding in the beam).

A total of 37 beams were tested. The measurements made in the tests included the deflection of the beam and the vertical acceleration of the load. In general, the results show that an increase in the load speed causes the beam deflections to increase, and the point of maximum permanent deflection to move toward the departure end. An increase in the load magnitude also causes an increase in the response, measured in terms of the corresponding static response.

In interpreting the data further, the maximum dynamic bending moment in the beam was estimated and compared with the static value of the moment carrying capacity. The behavior of the beam-load system was then explained in terms of the interrelations among the deflections, bending moments, curvatures, load speed, and load reaction. It is suggested that the centrifugal force of the moving load played a key role in the behavior.

In the following, Chapter II contains a description of the apparatus and instrumentation. The properties of the test beams and the test programs are described in Chapter III and Chapter IV,

respectively. The results of the experiments are discussed in Chapter V. An explanation of the overall behavior observed, together with a summary of this report, is presented in Chapter VI.

1.2 Notation.

The symbols used herein are defined in the text where they first appear. For convenience, the most important ones are summarized here in alphabetical order.

b = distance between point of maximum permanent set and entry end;

c = half of beam depth;

d = distance between position of maximum magnitude of moving force and entry end;

e = permanent deflection of midspan;

E = modulus of elasticity;

f = elastic fundamental frequency of unloaded beam;

g = gravitational acceleration;

I = moment of inertia;

k_y = elastic yield curvature = M_y/EI;

$(k_p)_a$ = average permanent curvature ;

$(k_p)_{max}$ = maximum permanent curvature;

L = span length of test beam;

M = maximum bending moment in beam at a given time;

M_f = final value of midspan moment in static test beam at "collapse";

M_u = ultimate moment = $(3/2)\ (\sigma_y I/c)$;

M_y = yield moment = $\sigma_y I/c$, (σ_y taken from tension tests);

n = a parameter, see Eq. 5.3;

$\bar{P}$ = $\frac{\text{(maximum magnitude of moving force on beam)}}{\text{(static value of moving load)}}$;

P = interaction force, or dynamic force on beam due to moving mass;

P_s = static carriage load on beam;

P_y = yield load for mid-span ($=4M_y/L$);

Q = mass of carriage;

t = time;

u = vt = distance between carriage and entry end;

v = speed of carriage;

$\ddot{w}$ = vertical acceleration of carriage;

y_c = maximum crawl deflection of midspan;

y_d = maximum mid-span deflection;

α = v/fL, speed parameter;

β = P_s/P_y, weight parameter;

σ_y = yield stress;

θ_1 = permanent angle of rotation of beam at entry support;

θ_2 = permanent angle of rotation of beam at departure support;

θ_p = total angle change or rotation of "plastic hinge".

II APPARATUS AND INSTRUMENTATION

2.1 General.

Fig. 2.1 shows a schematic diagram of the test set-up. The apparatus consists of a single-wheel load carriage which moves across a test beam. The load carriage is accelerated, prior to its entry upon the test beam, by the energy of a dropping weight. This energy is transferred to the load carriage by a system of wire ropes and sheaves. The acceleration and deceleration of the carriage takes place on an acceleration track and deceleration track, respectively. A load arrestor serves the purpose of stopping the carriage. The carriage is guided, mainly, by its monorail assembly which travels on a monorail guide track.

A linear variable differential transformer records the mid-span deflection history of the test beam. An accelerometer, located on the chassis of the carriage, measures the vertical acceleration of the load. An overall picture of the test set-up is shown in Fig. 2.2. Detail descriptions of the various parts are presented in the following.

2.2 Test Beams.

The design of the test set-up began with a choice of the material and size to be used for the test beams. Mild steel was chosen because of its relatively well-defined yield stress. A length of 2 ft. and a cross section 1/4 in. deep by 1 in. wide were chosen as a compromise between the considerations that (1) the size must be large enough to facilitate instrumentation, and

(2) it should be small enough so that the entire experimental system is manageable in the laboratory.

To facilitate attachment to the supports, the end faces of the beam were tapered at a 60 deg. angle from the horizontal. Thus the upper surface of the beam was 24 in. in length and the lower surface was 24.35 in. in length. The mechanical properties of the test beams will be discussed in Chapter III.

2.3 Beam Support System.

The beam support system may be seen in Fig. 2.3. First, clamps were attached to the ends of the beam by four set-screws. The clamps were, in turn, pin-connected to angle supports. The use of the clamps avoided drilling holes through the beam that might significantly affect the response. Furthermore, it facilitated easy installation and removal of the test beam --- a significant feature since there were many beams to be tested.

Dimensions of the clamps were 1 in. long by 1 1/2 in. wide by 3/4 in. deep. The beam rested in a slot in the upper surface of the clamp. The slot had a width and depth equal to that of the beam. A 1/4 in. diameter pin passed through a hole in the clamp. From the neutral axis of the beam to the center of the pin was a distance of 3/8 in. The center line of the pin was in the vertical plane containing the end width of the upper surface of the beam. Identical clamps were located at each end of the beam.

The pin passed through the clamp and extended on either side

where it was supported by a pair of support angles. Two support angles were found at each end of the beam. The two angles at one end of the beam were mirror images of each other. The pairs at each end were similar, but not exactly alike. The pair at the approach end allowed the support pin to translate horizontally and rotate, while the pair at the departure end allowed only rotation.

All support angles were made from 1-1/4 in. by 1-1/4 in. by 1/4 in. steel angle, 2 in. long. The horizontal legs were bolted to the "piers". The vertical legs of the approach pair had horizontal elongated slots in which the pins rested. Instead of having an elongated slot for the pin, the departure end angles had a 1/4 in. diameter hole which allowed pin rotation only. No vertical movement of the pin was allowed.

The horizontal legs of the angles had slots through which anchoring bolts passed. These slots facilitated the alignment of the test beam with the load tracks.

The angles were bolted to steel plates which, in turn, were connected to the top of the "abutments". The steel plates, 4 in. by 5 in. by 1/2 in., could be moved vertically in relation to the abutments. This allowed for adjustment of the vertical position of the test beam.

The abutments were made of concrete blocks and short pieces of steel wide flange section. The concrete blocks were bolted to the floor by brackets, and the wide flange pieces bolted to the top of the blocks.

2.4 Drive System.

The drive system consisting of a loop of wire rope around two sheaves, was activated by releasing a dropping weight from a tower. The tower was a 12 ft. tall structure fabricated from 1-1/4 in. by 1-1/4 in. by 1/4 in. angle bars. The weight was supported by a 1/4 in. diameter wire rope which ran to the top of the tower, across two sheaves, down the outside of the tower and connected with the upper strand of the loop.

The dropping weight consisted of from one to seven plates, each weighing 10 lbs., bolted together. The plates fell from a height of about 10 ft. The velocity of the carriage was varied by changing the number of plates.

The two sheaves of the drive pulley system (see also Fig. 2.1) were spaced 13 ft. apart and located in the vertical plane of the tracks above the monorail track. The upper branch of the loop of wire rope was tied to the wire rope from the tower. The lower branch had a fixture in the form of a small disk, which, prior to testing, was placed in contact with an extension of the roller assembly of the carriage. (See Section 2.6.)

At the tower base a trigger mechanism was located. When it was activated, the weight fell, and the disk pushed the carriage and accelerated it along the track. The drive pulley system was mechanically independent of the tracks.

The dropping weight landed on a platform located at the tower base. This platform was supported on four columns which passed through holes in the laboratory floor down to the basement.

There was no contact between the columns and the laboratory floor; thus the latter was isolated from the impact effect of the dropping weight. The platform was a steel grid covered with plywood and foam rubber.

At the end of the deceleration track was located a pneumatic stopping device. (See Fig. 2.5.) It consisted of a wire rope extending across the path of the carriage and by four pulleys down to an air cylinder bolted to the floor. Its purpose was to absorb the kinetic energy of the carriage.

2.5 Supporting Equipment.

Before and after the crossing of the beam, the carriage wheel ran over an acceleration track and deceleration track, respectively. These tracks were in the same vertical plane and at the same horizontal level as the test beam. The cross section was fabricated from 1 in. by 1 in. cold-rolled steel bar stock, to the sides of which was bolted 1/8 in. plates to form a guide trough 1/4 in. deep for the carriage wheel. The tracks were pin supported to piers similar to those described for the test beam supports.

In the same vertical plane and above the test beam level was the monorail guide track. It was a 1 in. by 1-1/2 in. aluminum beam extending the full length of the track. It was mounted on arms extending out and up from the webs of the wide flange piers. The roller hanger assembly of the carriage (see Section 2.6), ran on this guide track.

As previously noted, the acceleration track section provided a guidance trough for the carriage wheel. The test beam section did not. To ensure that the carriage stayed on the test beam, a 1/4 in. thick "guide plate", 2 ft. long, was mounted vertically to one side of the beam. (See Fig. 2.3) Two small arms with a roller attached at their ends and extending down from the carriage straddled the guide plate. If the carriage strayed from the center of the beam, the roller of either arm would come to contact with the plate and align the carriage. The guide plate would not restrict the forward or vertical carriage motion.

2.6 Load Carriage.

The carriage was designed to simulate a single axle load. Considerations which entered into its design include the following. First, the carriage had to be rugged enough to withstand repeated tests with weights up to 70 lbs. at speeds up to 16 fps. Secondly, it had to be stable in motion, although it had only one wheel. Thirdly, it had to function properly while undergoing large vertical deflections (≈2 in.).

The load carriage (Fig. 2.6) consisted of a chassis that supported a load box, and was mounted on a single wheel. The chassis was an aluminum frame which was supported at the leading end by a roller assembly, and at the trailing end by the single wheel.

The roller assembly consisted of a set of rollers mounted on

the top of a vertical bar that was attached to the monorail quide track. This bar was pin connected to the front of the chassis. The roller assembly was free to translate the length of the monorail guide track, but did not allow the vertical bar to rotate with respect to the track. The pin connection permitted the chassis to rotate in the vertical plane of the tracks. This rotation made it possible for the wheel at the rear of the chassis to move vertically.

The wheel, made of steel, was 3 in. in diameter and was connected to an axle by ball bearings. The carriage was balanced with weights at its leading end, so that the wheel was located at the center of percussion of the carriage (excluding the vertical bar). The total weight of the carriage when empty was 28.7 lbs. The corresponding rear wheel reaction was 19.6 lbs.

Approximately 4 in. behind the roller assembly, a vertical flat bar was hinged to the chassis. It was pin connected to another vertical flat bar attached to the roller assembly behind the main stabilizing bar. The pin connecting these two bars lay in an elongated slot in one of the bars. If the vertical deflection of the wheel became excessive (more than 4 in.), the pin engaged the end of the slot and further deflection was prevented. This was a safety feature to prevent damage to the carriage, and in no way hindered the operation of the carriage under normal deflections.

Centered directly over the carriage wheel was a steel, rectangular box supported by two leaf springs located on either side of the box and attached to the chassis. It should be pointed out that the carriage was designed to be used as a sprung load system. In such a system, the leaf springs would support the load box. To use the carriage as an unsprung load system, aluminum blocks were added between the leaf springs to restrain all motion of the load box relative to the chassis. Fig. 2.6 shows the aluminum blocks in place and the carriage as an unsprung system.

Lead plates of various weights were placed inside the box in order to change the weight of the carriage. Up to 60 lbs. of plates could be added to the box.

When the carriage was used as a sprung load system (no blocks added), the box was restrained from horizontal motion, relative to the chassis, by a rod and sleeve. The rod was anchored on the chassis, just ahead of the box. The sleeve was centered on the leading face of the box. As the box moved vertically, the sleeve moved on bearings along the rod. This arrangement allowed full vertical motion of the box with negligible friction.

2.7 Measurements and Recordings.

The major piece of equipment for measurements and recordings was a four channel Sanborne 150 Recording System, which furnished power to the measuring devices in addition to acting as the recording system.

Located at midspan of the beam was a Schaevitz Linear Variable Differential Transformer, Type No. 4000 XS-B, with a range of ± 4 in. Its purpose was to record a history trace of the vertical movement of the beam midspan.

To determine the velocity of the carriage, a microswitch was placed at the departure end of the beam. Examination of the history trace of the midspan deflection would reveal the time of entry of the carriage onto the beam. The microswitch indicated when the carriage left the beam. Knowing the beam length and paper speed, the average carriage speed was determined.

It was desirable to know the force applied to the beam by the carriage at any one time. To accomplish this, a Statham Accelerometer, Model No. AJ 43-15-350 with a range of ± 15 g's, was attached to the carriage chassis directly over the rear wheel. (See Fig. 2.7) This accelerometer measured the vertical acceleration of the carriage. The acceleration, together with the carriage mass, was used to calculate the interaction force between the beam and carriage.

III PROPERTIES OF TEST BEAMS

3.1 General.

As mentioned previously, the test beams had a rectangular cross section of 1/4 in. deep by 1 in. wide; the corresponding moment of inertia is equal to 0.0013 in.^{4}. They were 24 in. long and simply supported.

The beams were cut from hot rolled mild steel (C1095) bars (each about 20 ft. long). For a given test series, all specimens were taken from one bar stock.

3.2 Static Strength.

3.2.1 Yield Stress. For each test series, or a given bar, the (upper) yield stress was determined by the usual direct tension test. The results are summarized in Table 3.1. It is noted that the mean is of the order of 30,000 psi and the standard deviation is of the order of 600 psi.

3.2.2 Bending Moment-Curvature Relation. Eight static beam tests were made to obtain the moment curvature relation. A typical result is shown in Fig. 3.1, in which, the test arrangements are also depicted. The curvature was obtained by strain measurements at the top and bottom faces of the beam. In Table 3.2 are summarized the results of the eight tests. The symbol M_f denotes the final value of the moment applied to the mid-span of the test beam before it "collapsed". In this table are listed also the yield moment M_y and the ultimate moment $M_u = 1.5M_y$ as computed from the mean yield stress listed in Table 3.1. It

is seen that M_u is generally about 5% higher than M_f.

3.2.3 Discussion. Although the variations of the yield strength of the material used in this study are not unusual (say, of the order of 6%), it must be borne in mind that the experiments were to involve inelastic action, and the beams were statically determinate. Under these conditions, the response would be very sensitive to small variations of material properties as well as of loading.

3.3 Dynamic Properties.

3.3.1 Strain Rate Effects on Yield Stress. It is well known that the yield stress of mild steel increases with the rate of strain. For the tests made in this investigation, the maximum strain rate is of the order of 10^{-1} in./in./sec. (see Section 5.6). This would raise the yield stress by about 10% over the static values (see Ref. 6).

3.3.2 Natural Frequencies and Damping. The weight of the beam is 0.85 lbs./ft. The modulus of elasticity is 28×10^6 lbs./in.^{2} The fundamental (elastic) natural frequency of the test beam depends on whether the beam is loaded by the (moving) carriage, or not. If the beam is not loaded, the calculated frequency is 33.3 cps. This value has included the effect of the weight (0.27 lbs.) of the rod for the differential transformer at the midspan. The calculation is based on the Rayleigh Method by assuming a sinusoidal mode shape. The measured fundamental

natural frequency is 32.3 cps. The influence of higher elastic frequencies is considered negligible for this investigation.

Because of the ratio of the mass of the moving load to that of the beam (generally, about 30:1), the frequency of the loaded beam is much lower than for the unloaded beam. Considering a load of about 50 lbs. at the midspan, the loaded frequency is about 4 cps.

There is relatively little damping when the unloaded beam is vibrating freely. Assuming the usual viscous damping, the damping coefficient is approximately 2.5% of the critical.

IV TEST PROGRAMS AND PROCEDURES

4.1 Parameters Studied.

Two variables were studied in this investigation: the speed and the weight of the load. The speed is described in terms of the dimensionless parameter:

$$\alpha = v/fL \qquad (4.1)$$

in which, v is the speed, f is the elastic fundamental frequency of the beam, and L is the span length. Since fL is constant for all beams tested, the value of α is directly proportional to the actual load speed. The highest speed used in the study is 16.0 fps, which corresponds to a value of $\alpha = 0.20$. For simple span highway bridges, this would approximately correspond to 73 mph (5).

The weight of the load was considered in terms of the dimensionless parameter:

$$\beta = P_s/P_y \qquad (4.2)$$

where, P_s is the static carriage load on the beam and P_y is the "yield load" which, if placed at the midspan of the beam, would just cause yielding of the outer fibres of the beam. For each test series (involving specimens made from a single bar stock), the mean value of the yield stress, as listed in Table 3.1, was used to compute P_y. In this investigation, the values of β used varied from 0.9 to 1.3.

4.2 Test Program.

Four series of tests were conducted, each for one value of

β, for β = 0.9, 1.0, 1.2, and 1.3. Each series consisted of runs at different speeds. In particular, two "crawl runs" were made for each series. These runs corresponded to a sufficiently low speed such that the dynamic effects were negligible. The resulting midspan displacement was used as a reference for measuring the beam response to loads at higher speeds.

If a permanent set was recorded after a test, the beam would not be used again as another specimen. If no permanent set was observed, the beam was considered undamaged and would be used as a test beam again. A total of 37 beams were used in this investigation.

4.3 Test Procedures.

The procedure followed during the testing may be described as follows. The accelerometer and differential transformer were calibrated before the start of the testing. After the calibrations were completed, a test beam was placed. Prior to making any runs, checks were made to see that the beam was aligned horizontally with the tracks and vertically with the monorail. This was accomplished by the use of a taut string over one edge of the beam and tracks, and a plumb bob suspended from the monorail track down to the beam.

Particular care was given to render a smooth entry of the carriage to the beam. The gap between the entry end of the beam and the acceleration track was made as small as possible without allowing them to actually come to contact. The elevations of the

ends were adjusted to be as nearly equal as possible. These fine adjustments were judged by eye and the touch of the fingers.

After the above calibrations and adjustments, the dynamic test runs were performed. With the paper speed of the recording system set at 100 mm/sec., recordings of midspan deflection and carriage acceleration were made. Deflections of crawl runs were recorded at a paper speed of 20 mm/sec.

V RESULTS OF INVESTIGATION

5.1 General.

The results of this investigation will be presented according to the following scheme. First, the "typical behavior" of the beam-load system will be described based on an examination of a Sanborn record of the time histories of the mid-span displacment of the beam and the vertical acceleration of the moving load. Observations on the general phenomena from multi-exposure photographs and motion pictures will also be made.

Next, the quantitative effects of the speed and the magnitude of the moving load are discussed. The quantities considered are the maximum mid-span deflection, the maximum permanent set, and the maximum interactive force between the beam and the load. All these quantities were directly measured during the experiments.

The data are then further interpreted, now frequently aided by engineering judgment, so that some estimation of the magnitude of the maximum dynamic bending moment can be made, and the interactions among the dynamic forces, bending moments, curvatures, and displacements may be related.

5.2 Typical Behavior.

5.2.1 Sanborn Records. The records presented in this section may be considered qualitatively as typical of the behavior of the beam-load system in all tests performed. Quantitative

aspects of the test results are discussed in subsequent sections. In Fig. 5.1, a Sanborn recording of a test run for $\beta = 1.0$ and $v = 14.7$ fps is presented.

The top trace in this figure represents the mid-span deflection of the beam. It shows that at the time the carriage enters the beam, almost immediately, there is a downward movement of the mid-span. This downward deflection continues to increase as the carriage moves over the beam, even after the carriage has passed the mid-span. The maximum deflection, y_d, equal to 0.815 in., actually occurs when $u = 0.85L$, where u denotes the distance between the carriage and the entry end of the beam.

While the load is on the beam, the elastic vibrations are seen to be small. As the carriage leaves the beam, the structure rebounds suddenly and then vibrates violently, apparently in an elastic manner, centering upon a new equilibrium position. This new position corresponds to that of the permanent set, as may be seen after the vibrations have been damped out. The set, e, is equal to 0.078 in.

The bottom trace in Fig. 5.1 is a record of the vertical acceleration of the carriage. The vertical acceleration of the carriage, $\ddot{w}$, determines the dynamic force on the beam according to the equation:

$$P = Q(g - \ddot{w}) \qquad (5.1)$$

where, P is the dynamic force on the beam due to the moving mass; g is the gravitational acceleration; and Q is the mass of the

moving carriage. Since the carriage mass and the gravitational acceleration are constant, the force on the beam is directly proportional to the acceleration of the carriage.

As the carriage enters the beam, the acceleration quickly becomes positive (downward) with a value of approximately 0.6g. This results in a dynamic force of only about 0.4 times the static value. The acceleration begins to decrease algebraically at $u \cong L/4$. The rate of the decrease is apparently very high (see Eq. 5.2 for an approximating mathematical expression), lowering the acceleration to a minimum of -5.1g. This decrease in acceleration represents an increase in the dynamic force on the beam. The force reaches a maximum value at $u = 0.93L$, a position that is even closer to the departure end than that corresponding to the maximum mid-span deflection. The maximum force is 5.1 + 1 = 6.1 times the static value. The corresponding bending moment under the load is 520 inch-pounds; the static ultimate moment carrying capacity is about 470 inch-pounds.

After the minimum, the acceleration increases even faster than it has previously decreased. Within the short interval between $u = 0.93L$ and $u = 1.0L$, it has increased from -5g to 0g. After leaving the beam, the carriage acceleration is erratic. But the positive one g value recorded immediately after the departure is interpreted to be due to the fact that the carriage, moving past the departure end of the beam, momentarily lost contact with the following load track and falls freely in the air. Further large values are probably due to the restrain-

ing force offered by the hanger bar of the carriage as its upward movement becomes excessive. (See Sec. 2.6.)

5.2.2 Multiple-Exposure Picture. In Fig. 5.2, a multiple exposure picture of the travel of the carriage is presented. The picture was taken at a rate of 8,000 exposures per minute. This picture and the previously described Sanborn recording are of the same test run.

The lower level of dots show the trajectory followed by the axle of the carriage wheel as it moved across the beam. The smoothness of the trajectory indicates relatively little elastic vibration of the beam. The even spacing of the dots, except near the departure end of the beam, shows the nearly constant speed of the carriage during the crossing. The maximum ordinate of the trajectory is seen to occur at about the third quarter point, and the maximum curvature appears to be even beyond that point. The shapes of the beam prior to and after the test run can be seen also. These two shapes result from exposure of the beam at equilibrium before testing, and at equilibrium after the motion has been damped out. Initially, the beam is seen to be straight. After the passage of the carriage, the beam exhibits a definite "kink" in the neighborhood of the third quarter point. This kink or "plastic hinge" actually results from a continuous distribution of relatively large curvature over a finite length of the order of 6 in. The beam is straight on either side of the hinge. This mode of deformation was present in all tests, in which, permanent set

occurred. (See also Fig. 2.3.)

5.2.3 Motion Pictures. As a further independent observation of the behavior of the beam-carriage system, motion pictures of several test runs were taken, using a Fastax high speed camera. Evidence from the film corroborates the statements presented in the previous two sections.

5.3 Maximum Mid-Span Deflection.

The maximum mid-span deflection will be discussed in terms of the "amplification factor", y_d/y_c, in which, y_c denotes the maximum crawl deflection (for the same value of β, of course). For the case $\beta = 1.3$, the amplification factor is plotted in Fig. 5.3 as a function of the load speed. It is seen that the amplification factor increases approximately linearly with speed from 1.5 at $v = 6.4$ fps to 3.2 at $v = 16.0$ fps.

The curve in this figure is fitted "by eye" through the actual data points to represent the over-all pattern of the behavior. To compare the results for different values of β, such curves are plotted together in Fig. 5.4. The individual data points are not plotted in order to avoid cluttering the illustration. (They can be obtained from Table 5.1.) For all values of β an increase in v results in an increase in the amplification factor. Also, in general, an increase in β increases the amplification factor.

Two curves are given for $\beta = 1.2$: one from the S-4 series, one from the S-5 series. The S-5 series in seen to be somewhat off the general trend. One reason is felt to be the wide varia-

tion of yield stresses for this group of steel beams. (See Table 3.1) The actual material used in the dynamic tests may have been appreciably stronger than the average strength used in reducing the data.

5.4 Maximum Permanent Set.

Shown in Fig. 5.5 are the midspan permanent sets given in terms of y_c for $\beta = 1.3$. As expected, the set increases with speed, from 0.0 at v = 9.6 fps to 1.7 at v = 16.0 fps. In Fig. 5.6, are presented the general trends for $\beta = 1.2$ also. For smaller values of β, the magnitudes of the permanent set are too small to be plotted. However, they are listed in Table 5.1. It is seen that the magnitude of these permanent sets increases rapidly with the value of β.

The location of the maximum permanent set on the beam is shown in Fig. 5.7, in which the distance, b, between the point of maximum set and the entry end, is plotted against v. It is seen that except for the point corresponding to v = 16.0 fps, there seems to exist a trend that with increasing v the point of maximum set moves toward the departure end. It should be pointed out that the curvature (over a plastic hinge length of about 6 in.) is usually small and the point of maximum deflection cannot be conveniently determined precisely. In passing, it might be pointed out also that the point of maximum deflection does not necessarily coincide with the point of the maximum curvature, although they are close. This will be discussed further in a later section.

The trend of increasing values of b with increasing v is much more apparent for other values of β as is shown in Fig. 5.8. The other data points are tabulated in Table 5.1.

5.5 Maximum Magnitude of Moving Force on Beam.

Denoting by $\overline{P}$ the ratio of the maximum magnitude of the moving force on the beam to the static value of the moving load, in Fig. 5.9, is plotted, for $\beta = 1.3$, $\overline{P}$ versus v. The value of $\overline{P}$ is obtained by adding one g (the static force) to the maximum ordinate of the acceleration diagram, such as the bottom trace in Fig. 5.1, and dividing the sum by g. It is seen that $\overline{P}$ increases very rapidly with the velocity, at v = 13.6 fps, $\overline{P} = 8$. The data points for v = 14.4 fps and 16.0 fps are not shown, since the maximum accelerations were not distinctly recorded as the recording stylus was moving too fast, leaving too light a mark. As can be seen from Fig. 5.10, the same general trend holds true for other values of β.

The distance, d, from the entry end to the position of the maximum magnitude of the moving force is plotted in Fig. 5.11. A clear trend is seen of increasing values of d with increasing load speed. It is of interest to note that at v = 16.0 fps, the maximum occurs when the load is only less than one-tenth of the span to the departure end. Similar plots for other values of β show the same trend, but are not presented here.

5.6 Estimation of Maximum Bending Moment.

5.6.1 Approximate Mathematical Representation of the Moving

Force. In order to estimate the maximum bending moment, it is necessary to obtain an expression for the moving force. A study of the acceleration records indicates that the moving force could be approximated by the following expression:

$$P \doteq P_o + c'P_s(u-h/L)^{n'} \qquad (5.2)$$

in which, P_o, c', h and n' are parameters, and P_s denotes the static load. Values of these parameters can be determined from the acceleration records by curve fitting techniques. When the moving load is close to the departure end, the first term P_o is small and h is small as compared to u. Thus, for sufficiently large u, P can be further approximated by:

$$P \doteq cP_s\,(u/L)^n \qquad (5.3)$$

in which, c and n are parameters determinable by curve fitting.

As mentioned previously, the rate of increase of $\ddot{w}$, hence, the moving force, increases with speed. This rate could be measured by the values of n which have been determined from a log-log plot of the data. In Fig. 5.12 is plotted n versus α which indicates the trend.

5.6.2 Location of Maximum Moment. Realizing that the inertia force of the beam is relatively small, it is reasonable to assume that at a given time the maximum bending moment, M, occurs at the section where the load is instantaneously located. Therefore, M is given by:

$$M = Pu(1 - u/L) = Pvt(1 - vt/L) \qquad (5.4)$$

in which, u = vt and t denotes time. Substituting Eq. 5.3 into Eq. 5.4 and taking the time derivative, one obtains:

$$dM/dt = P_s v[(n+1) + (vt/L)(n+2)] \qquad (5.5)$$

Setting this equal to zero and solving, the time, or load position, of the maximum moment that the beam has experienced during the passage (subsequently simply referred to as the maximum moment) is given by the following expression:

$$(vt/L)_M = (u/L)_M = (n+1)/(n+2) \qquad (5.6)$$

The preceding expression for the location of the maximum moment is derived from an analytical expression for the moving force, formed from observations on the carriage acceleration records. It is of interest to compare this location with the position of maximum permanent curvature of the actual deformed shape of the tested beam. However, it is difficult to determine accurately the point of maximum curvature of the deformed beam. But for a simply supported beam with a single "plastic hinge", as shown in Fig. 5.13a, the location of maximum permanent curvature is close to that of maximum deflection. Hence, the position of maximum permanent set observable from the tested beam is plotted in Fig. 5.14 together with Eq. 5.6.

It is seen that although the data points follow the general trend indicated by Eq. 5.6, all points lie below the analytical curve. Of course, there could be a number of reasons for this. For example, the inertia force of the beam is neglected in the discussion. (This effect is probably small; recalling that the

ratio of the moving mass to the mass of the beam is approximately 30:1.) The main explanation is thought to lie in the difference of the two quantities considered, i.e., one related to the maximum deflection and the other to the maximum curvature.

As implied before, the maximum deflection points and maximum curvature points, although close, do not actually coincide. Referring to Fig. 5.13, a and b, it is seen that the maximum deflection occurs at a section where the area under the (permanent) curvature diagram balances out the end slope, θ_1, (which by the "conjugate beam theorem" is equal to the "reaction" at the left-hand support; see Fig. 5.13b). It is not difficult to show that the point of absolute maximum moment is always closer to the departure end than the point of maximum deflection, provided that the curvature diagram meets the following two conditions. It has only one relative maximum, and its centroid does not lie closer to the departure end than its maximum. (In Ref. 7 are given curvature diagrams of plastic hinges due to moving loads. They all seem to satisfy the above conditions.) Assuming a 6-in. hinge length, with an equilateral triangular curvature distribution centered at the third quarter point, the point of maximum moment would be 0.88 in. or 0.0366L closer to the departure end than the point of maximum deflection.

5.6.3 Comparison of Maximum Moment vs. Static Capacity Moment. Assuming that the maximum moment occurred at the same section as the maximum permanent set, one can compute the maximum bending

moment from the load acceleration record. The values are listed in column 9 of Table 5.2. They vary from 576 in.-lbs. to 731 in.-lbs. According to static beam tests and/or tension tests (see Table 3.2), the static moment capacity is about 470 in.-lbs. Thus, the maximum dynamic moment varies from 1.22 to 1.55 times the static capacity.

The differences may be accounted for in part, at least, by two factors: the influence of strain rate effect on yield stress, and that of strain hardening. Based on Eq. 5.3, the time derivative of the bending moment at a fixed section, $x = k'L$, for the case $u = vt \geq k'L$ is:

$$dM/dt = -k'vP[1+n(1 - L/vt)] \qquad (5.7)$$

For $k' = 3/4$, $v = 120$ in. per sec., $P = 200$ lbs., $L/vt = 4/3$, the strain rate at the extreme fiber is of the order of -0.02 per in. to 0.06 per in. for $n = 2$ to $n = 6$, respectively. In either case, the yield stress would vary only about 10% of the static value. (See Ref. 6).

Strain hardening, if present, will undoubtedly increase the moment capacity. Whether it did exist may be estimated from an examination of the curvature distribution over the length of the plastic hinge. This is included in the next section.

5.7 Curvature and Centrifugal Force.

5.7.1 Estimation of Curvature. Referring to Fig. 5.13a, it is seen that the total angle change or rotation of the "hinge" is $\theta_p = \theta_1 + \theta_2$. The rotation can be approximated by the quantity:

$$\theta_p \tilde{=} 2e/(L-b) \qquad (5.8)$$

This expression generally underestimates the value of θ_p. For the order of magnitude of the quantities involved in this study, the error is approximately 10%. Assuming a hinge length of 6 in., one can estimate the average permanent curvature $(k_p)_a$. The values of θ_p and $(k_p)_a$ for the $\beta = 1.3$ series are listed in columns 3 and 4, respectively, in Table 5.2. In column 5 of the same table is listed the maximum permanent curvature, (k_p)max., taken as twice the average value (this seems reasonable in view of the data in Ref. 7 mentioned previously.)

Since the permanent curvature necessarily corresponds to zero bending moment, the maximum curvature that had been attained at the section could be obtained by drawing a straight line from the point of zero moment and permanent curvature with a slope parallel to the elastic line as shown in Fig. 5.15. (See Ref. 8.) The intersection marks the maximum curvature. Thus,

$$k_{max} = (k_p)_{max} + ck_y \qquad (5.9)$$

where, k_y is the elastic limit curvature and equals M_y/EI (EI is the elastic bending rigidity), and c varies from 1 to 1.5 assuming no strain hardening (i.e., assuming the "ultimate moment" $M_u = 1.5\ M_y$); with strain hardening, the value of c could be larger.

For a rectangular cross section in bending, it was shown in Ref. 8 (or see also Fig. 5.15) that strain hardening could begin when $k = 9\ k_y$. Hence, for the two tests; S-2-9 and S-2-6, the material has gone into the strain hardening region. However,

the increase in moment capacity due to the amount of strain hardening could only account for about a 15% increase.

Hence, on the average one could account for a 10% increase in moment capacity due to strain rate effects, and a 15% increase due to strain hardening for cases involving larger permanent sets. These percentages are not sufficient to explain the discrepancies between the approximate maximum dynamic moment and the static moment carrying capacity.

It might be mentioned that other possible causes of discrepancy could be the effect of inertia forces and shear effects and also experimental error. The inertia effects of the beam could make a maximum difference of about 5%. The shear effects are negligible. Thus, the dynamic ultimate moment could be 1.30 to 1.35 time the static ultimate moment. Variation in material properties could yield another 10% difference, leaving a discrepancy of 10% to 20% static ultimate moment unaccounted for. This is probably due to the unavoidable error involved in measurements and calibrations.

It is also entirely possible that the preceding approach may not be adequate to explain the inelastic dynamic phenomenon being considered here as the strain-hardening effects are based on a static theory.

5.7.2 Estimation of Centrifugal Force. From the estimated maximum curvature, k_{max}, one can easily calculate the maximum centripetal acceleration, which is equal to $v^2 k_{max}$. The ratio $(v^2 k_{max} + g)/g$ of course, represents part of the maximum dynamic force in terms of the static force. The values of this ratio are listed

in column 8 of Table 5.2. They are also plotted in Fig. 5.9.

It is recalled that the curve presented previously in this figure is from direct force measurements (acceleration). The one just introduced results essentially from displacement measurements. It is seen that they correlate reasonably well. One may thus conjecture that the essential feature in the phenomena observed is one of interplays between the bending moment, curvature and centrifugal force. This will be discussed further in the next chapter.

It should be pointed out that the curve corresponding to force measurements is more accurate, since it is a direct measurement of acceleration, but the estimated values are based on a number of assumptions such as the maximum curvature is twice the average curvature and, furthermore, the average speed is used while the speed at the departure end is generally lower than the average speed.

VI CONCLUSION

6.1 Basic Phenomena.

From the discussions in the preceding chapter, the behavior of the beam load system may be explained as follows. As the load moves on the beam, the load vertical acceleration lowers because of local beam downward acceleration. As the load moves further on toward the mid-span, at the point of contact the beam picks up curvature (due mainly to an increase in the bending moment), this results in an appreciable centrifugal force on the beam. This increased force causes greater curvature and deflection. The increase in curvature and in force feed on each other and continue to build up until the mass is near the departure end. There, because of the boundary condition, the curvature has to go to zero. Thus, the load drops--rather suddenly, too. The higher the speed is, the closer the point of maximum force is pushed toward the departure end.

It might be pointed out that even if the interaction force increases hyperbolically (as $L/(L-u)$), the bending moment would remain quite finite. If the reaction force starts to increase from the static value at the mid-span hyperbolically to infinity at $u = L$, the bending moment at the mid-span will be constant. At any given time, the moment is a maximum at the section instantaneously under the load. Its magnitude increases lineally as it moves toward the departure end attaining a maximum value equal to twice the moment at the mid-span. From the above, obviously the

maximum bending moment will occur at a point beyond the mid-span because, first, the influence line for mid-span moment is symmetric about the mid-span, and second, the moving force is larger after passing the mid-span.

After the mid-span, the magnitude of the bending moment under the load, as affected by the load position, is pulled by two opposing influences:

(1) As vt increases, the interaction force would increase, and thus tend to increase the bending moment.

(2) On the other hand, the statics or equilibrium condition of the beam requires that the moment drop to zero at the support.

Thus, as the interaction force increases at a faster rate, the point of maximum moment under the load will tend to move nearer to the departure end. Yet, at the end it must drop to zero. Thus, near the end the changes in bending moment under the load must be sharp and so would be the curvature. This also explains the sudden changes in the measured load acceleration representing the interaction force.

In the preceding description, only the geometry of the deformed beam and equilibrium conditions are explicitly involved; the material properties of the beam are not mentioned. Of course, the geometry of deformed beam implicitly involves the material properties. Therefore, the inelastic action would increase the deformation--hence, the curvature--and would essentially accentu-

ate the features of the general phenomena.

6.2 Summary.

An experimental study of the dynamic inelastic behavior of simply supported beams under heavy moving unsprung loads is reported. A total of 37 mild steel beams were tested in the investigation. The beams were 1/4 in. deep by 1 in. wide and 2 ft. long.

The load was in the form of a single-axle unsprung carriage propelled by the energy of a dropping weight to speeds varying from 6 to 16 fps. The weight of the load was varied from 0.9 to 1.3 times the mid-span yield load which is approximately 60 lbs. The mid-span deflections of the beam and the vertical accelerations of the load were recorded in the tests.

It was found that although loads heavier than the yield load could cross the beam, the permanent set increased rapidly as the load increased beyond the yield load. Generally, an increase of the speed of the crossing load causes a rapid increase in the damage. An analysis of the data indicates that the essential feature of the phenomena lies in the interplay of the curvature, the interacting force, and the bending moment.

LIST OF REFERENCES

(1) Parkes, E.W., "How to Cross an Unsafe Bridge," Engineering, Vol. 186, November, 1958.

(2) Symonds, P.S., Neal, B.G., "Travelling Loads on Rigid-Plastic Beams," Journal of Engineering Mechanics Division, ASCE, Vol. 86, No. EM1, January, 1960.

(3) Toridis, T., "Dynamic Behavior of Elasto-Inelastic Beams Subjected to Moving Loads", Ph.D. Thesis, Civil Engineering Department, Michigan State University, September, 1964.

(4) Luthe-Garcia, R., Walker, W., and Veletsos, A.S., "Dynamic Response of Simple-Span Highway Bridges in the Inelastic Range", Civil Engineering Studies, Structural Research Series, No. 287, University of Illinois, December 1964.

(5) Wen, R.K., Veletsos, A.S., "Dynamic Behavior of Simple-Span Highway Bridges," Bulletin 315, 1962, Highway Research Board, Washington, D.C.

(6) Manjoine, M.J., "Influence of Rate of Strain and Temperature on Yield Stresses in Mild Steel", Journal of Applied Mechanics, Vol. 11, No. 4, 1944.

(7) Wang, S.T., "Inelastic Behavior of Two-Span Continuous Beams Subjected to Moving Loads", M.S. Thesis, Civil Engineering Department, Michigan State University, September, 1964.

(8) Hodge, P.G., "Plastic Analysis of Structures", McGraw Hill, New York, 1959.

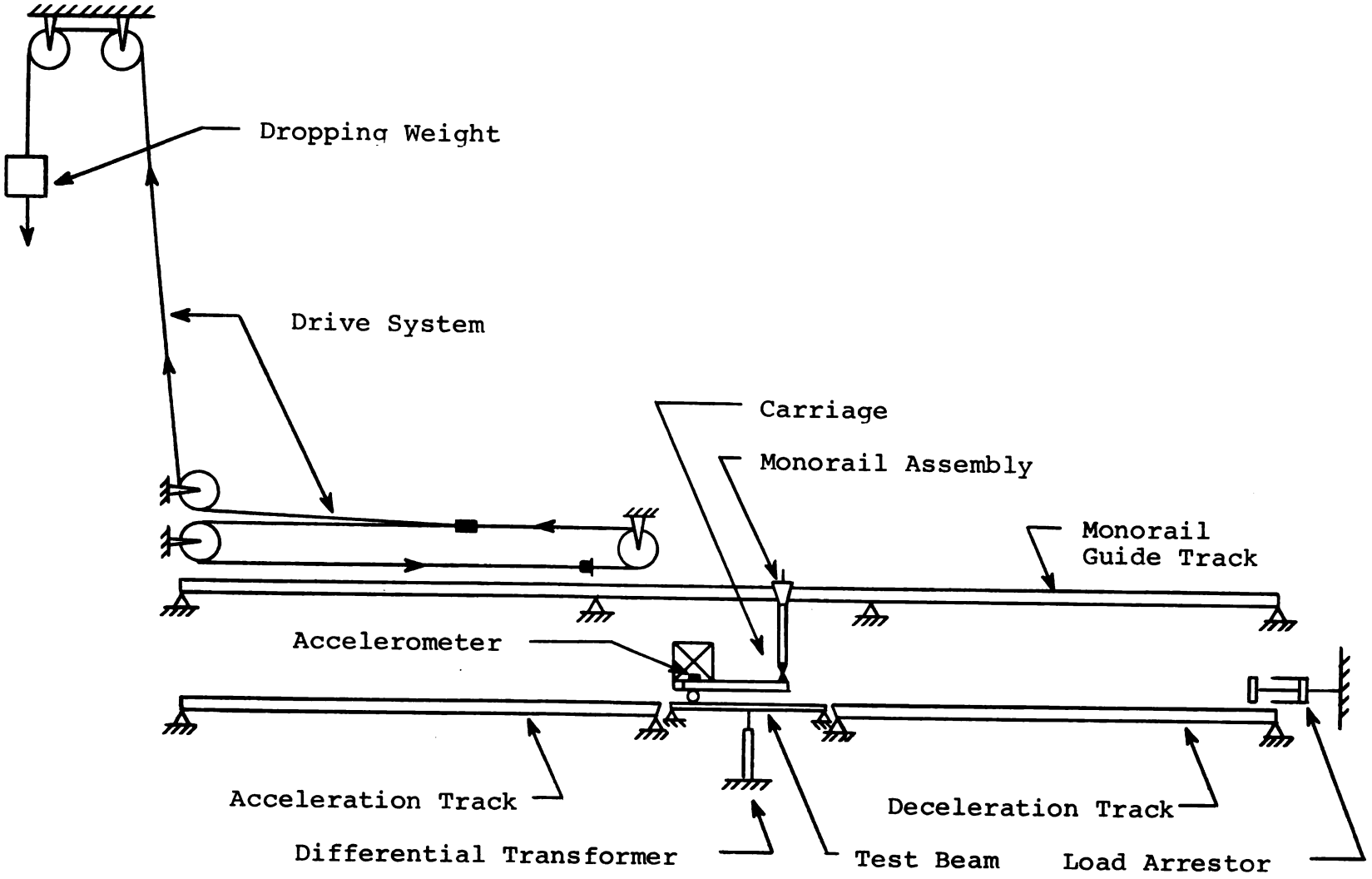

FIG. 2.1 SCHEMATIC DIAGRAM OF TEST APPARATUS

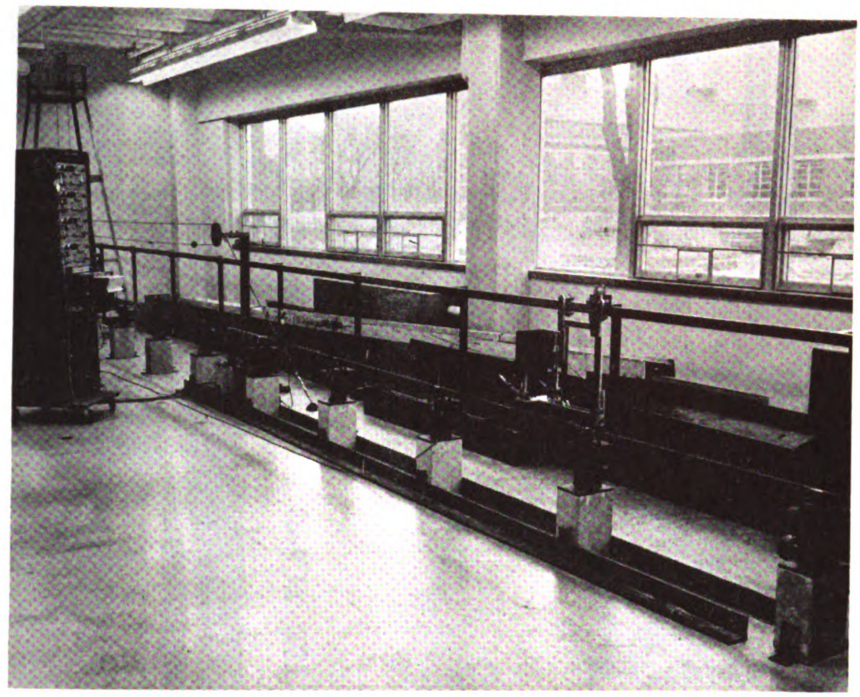

FIG. 2.2 OVERALL VIEW OF TEST SET-UP

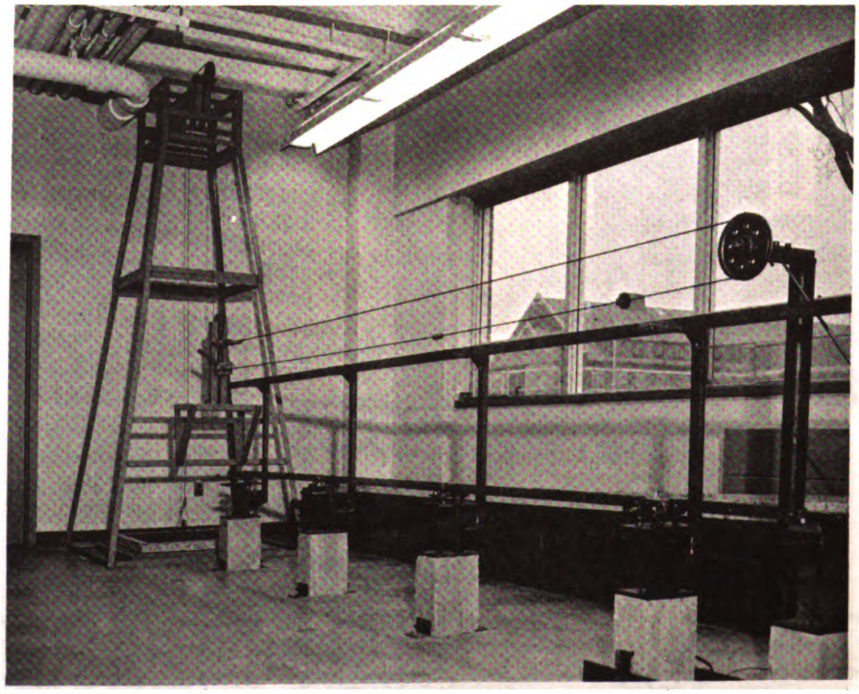

FIG. 2.4 DRIVE SYSTEM

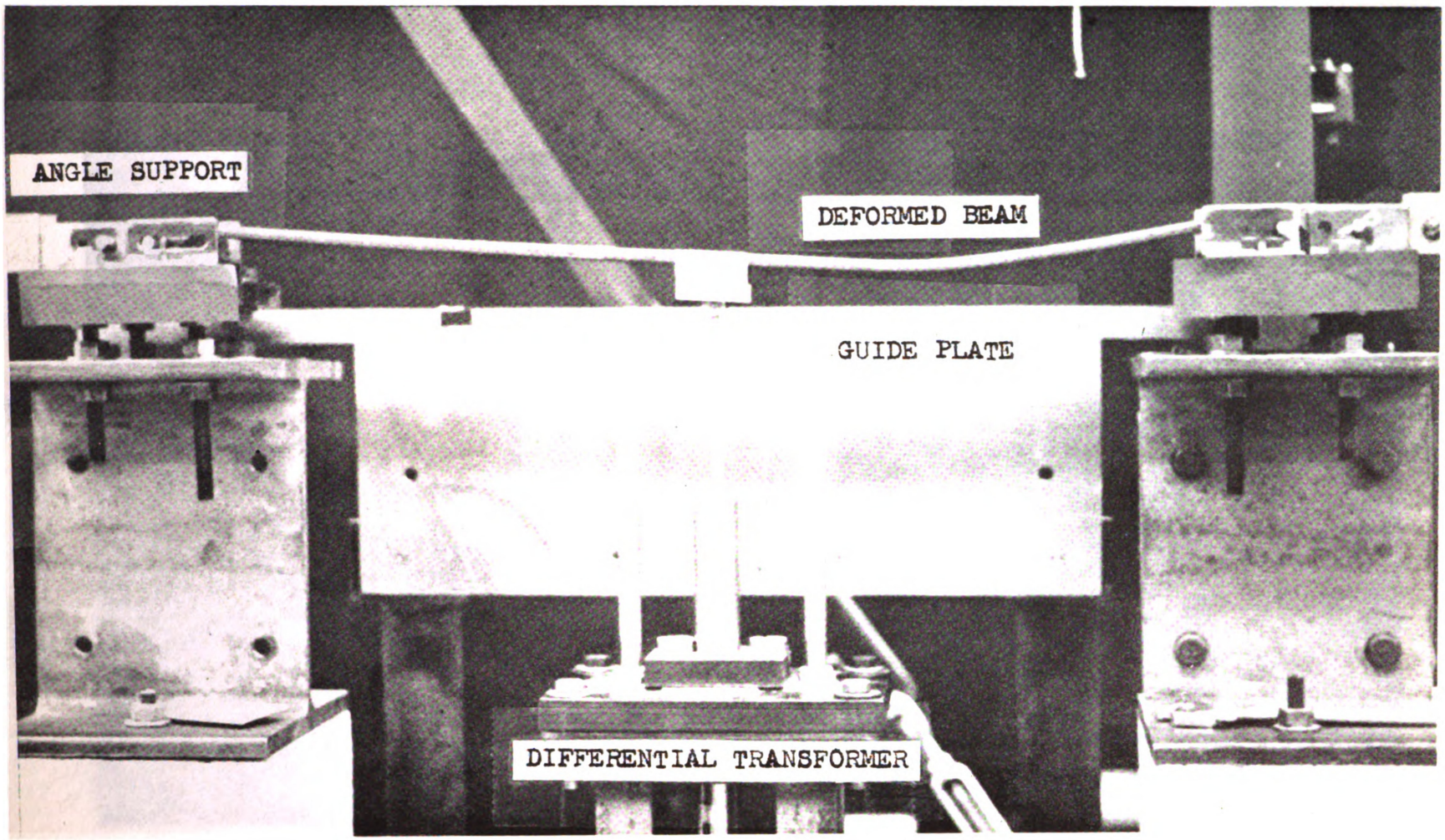

FIG. 2.3 TEST BEAM, SUPPORT SYSTEM AND DIFFERENTIAL TRANSFORMER

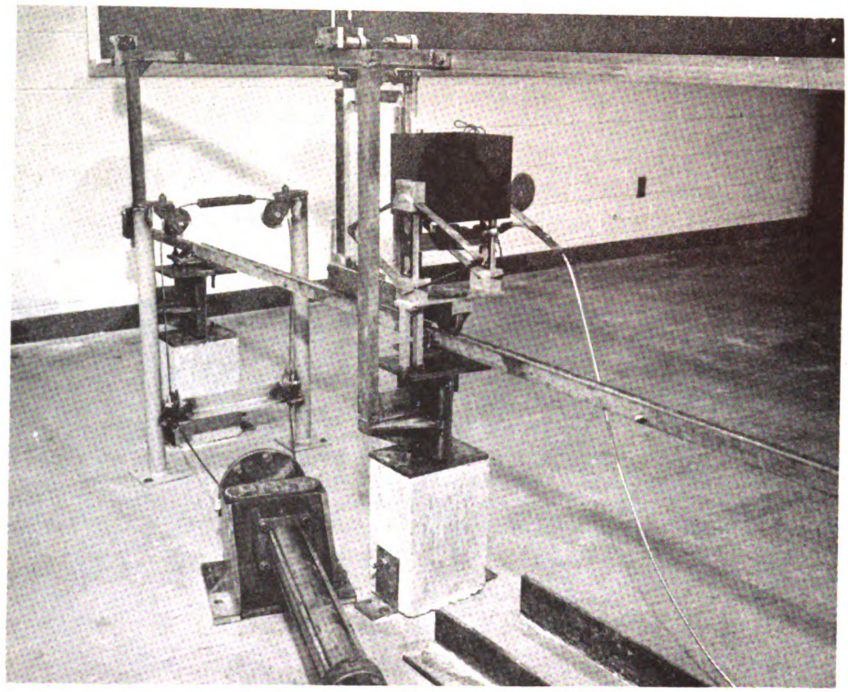

FIG. 2.5 LOAD ARRESTOR

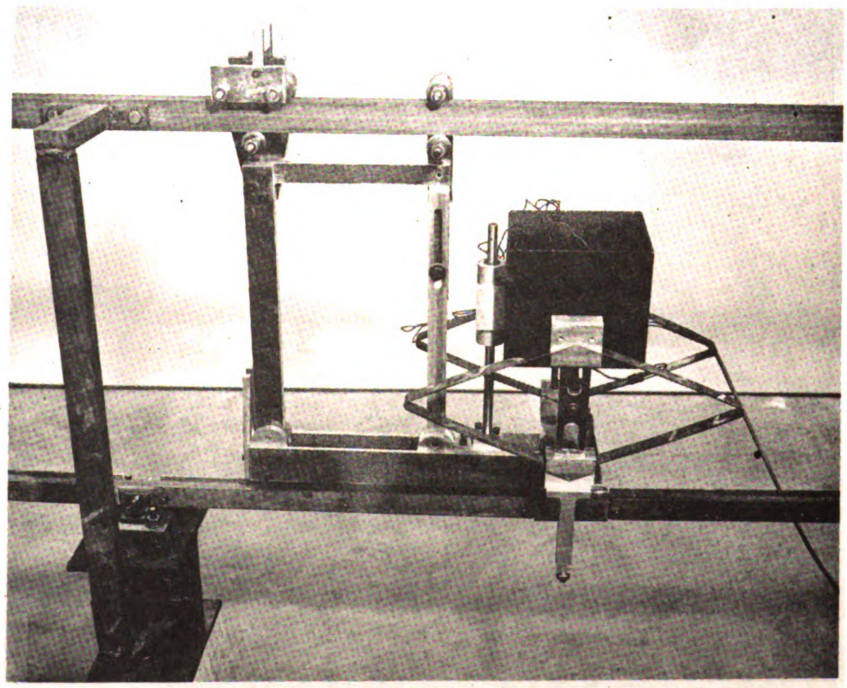

FIG. 2.6 LOAD CARRIAGE

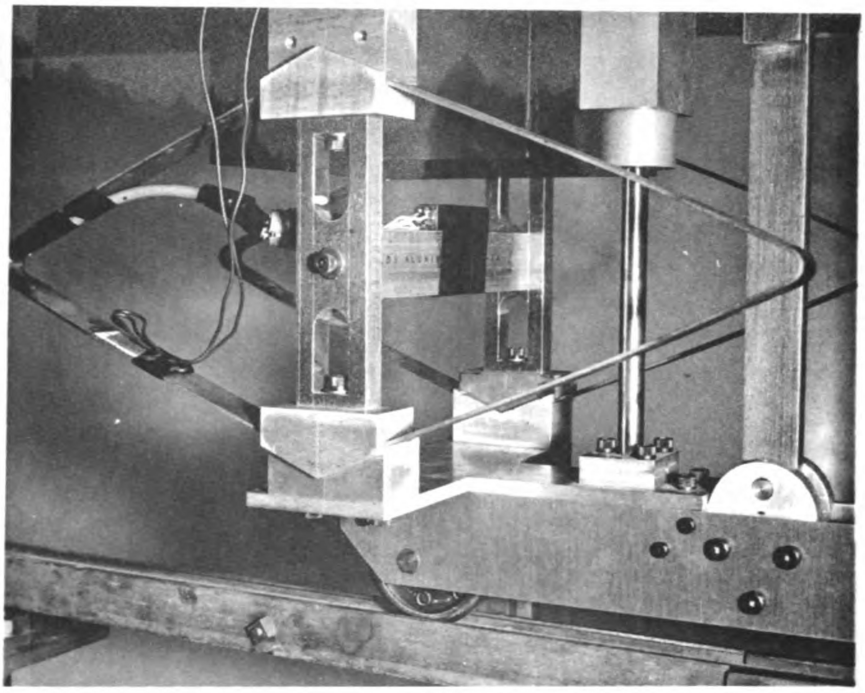

FIG. 2.7 ACCELEROMETER ON CARRIAGE

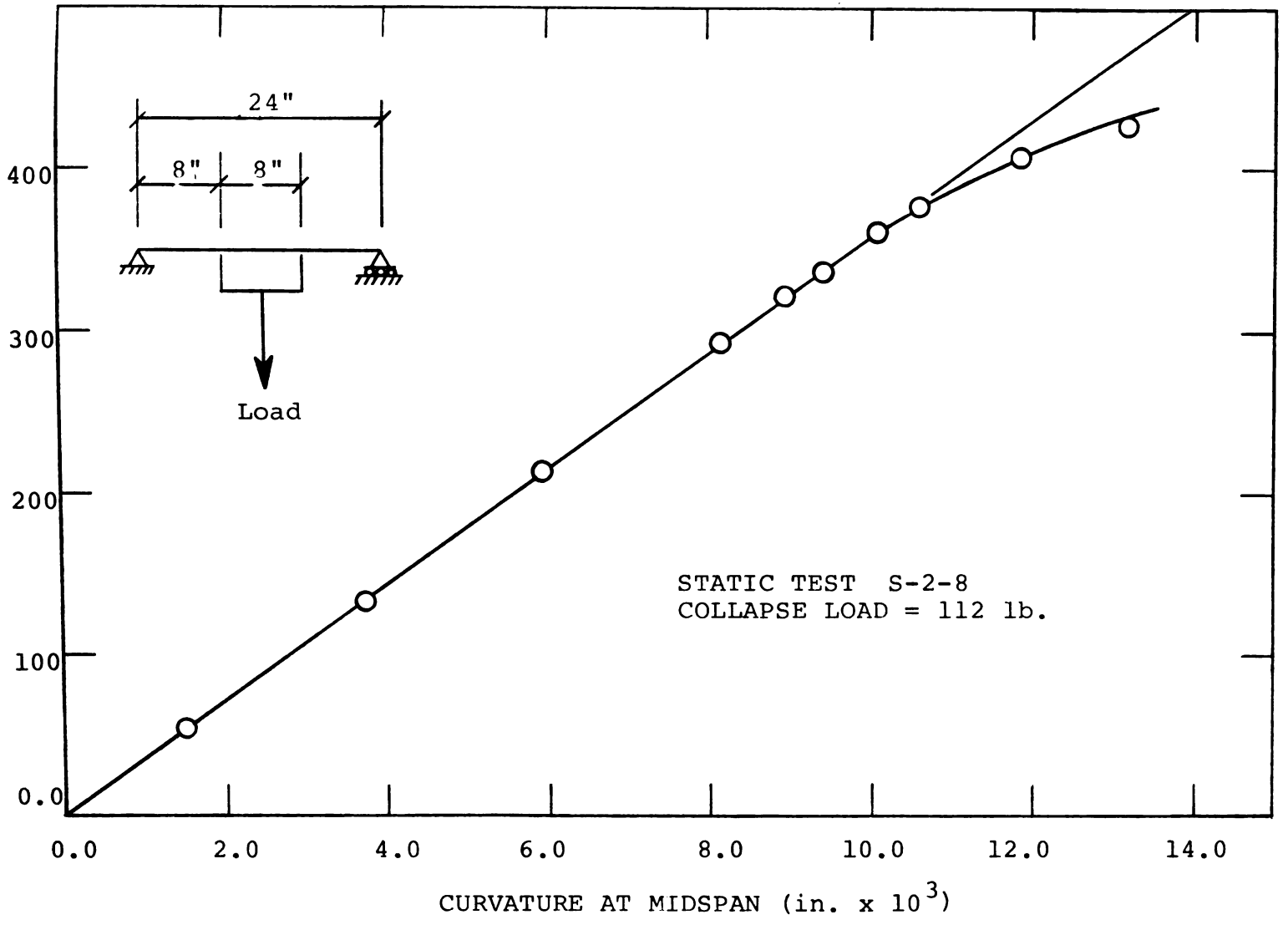

FIG. 3.1 MOMENT-CURVATURE RELATION

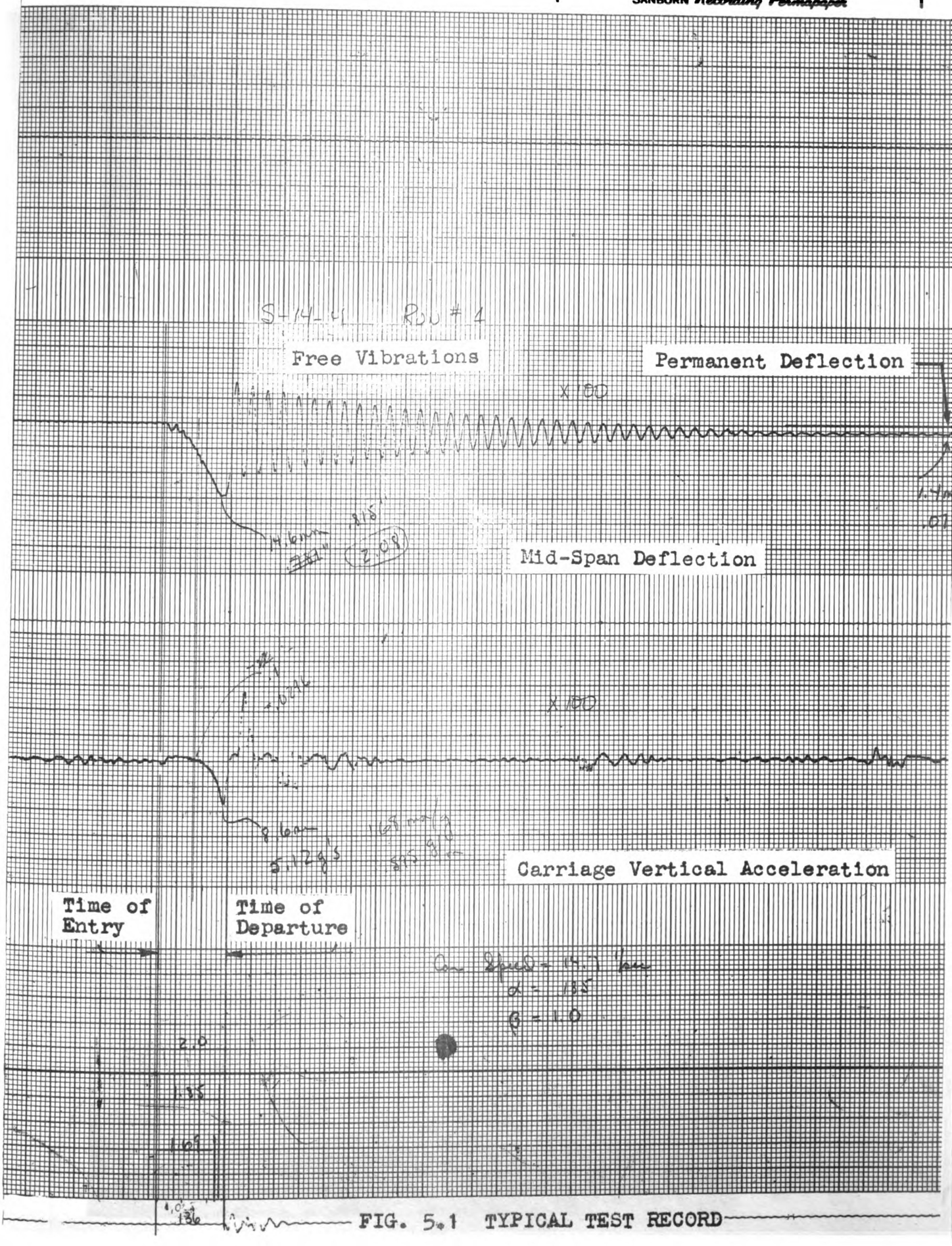

FIG. 5.1 TYPICAL TEST RECORD

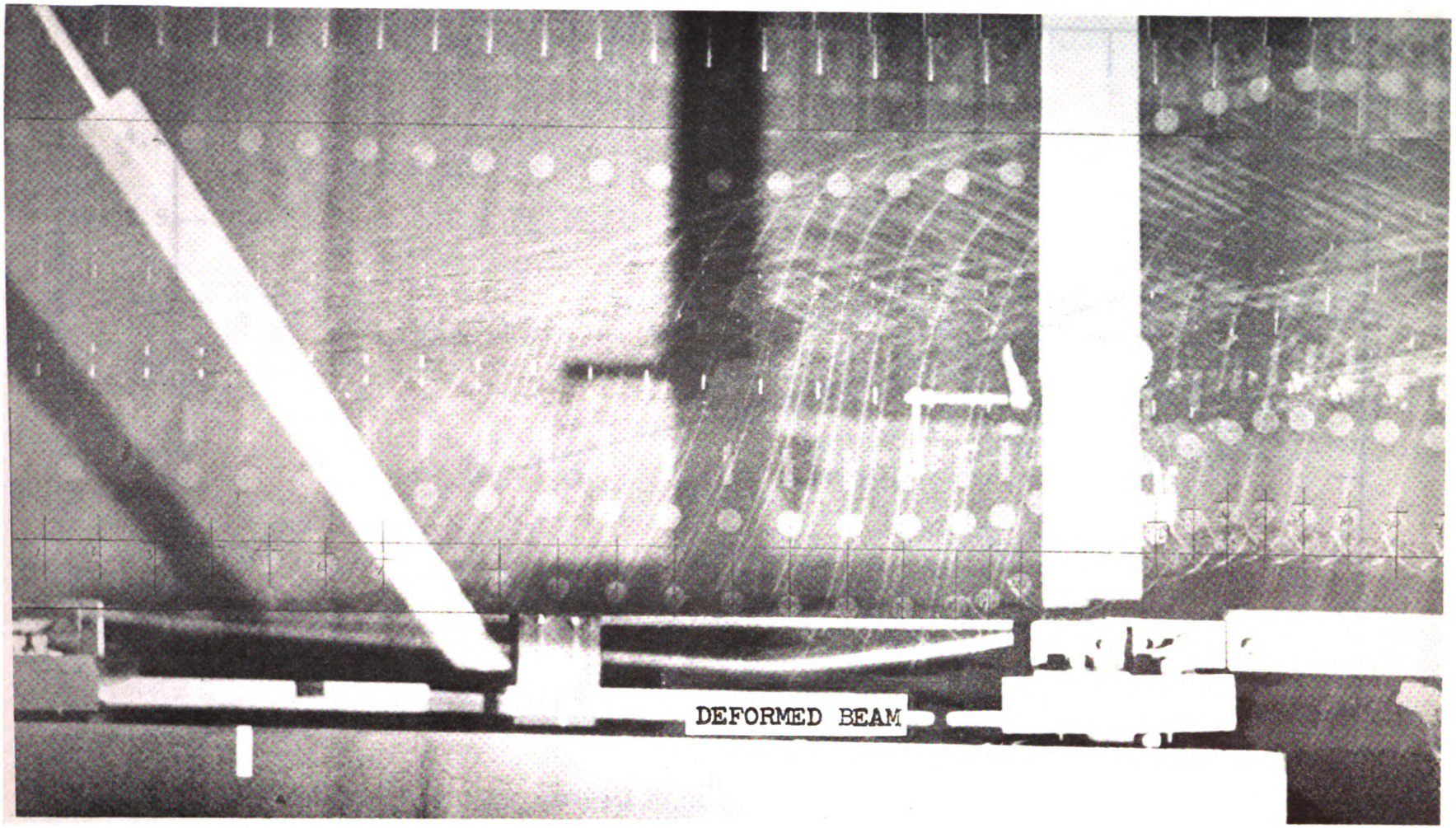

FIG. 5.2 MULTIPLE-EXPOSURE PICTURE

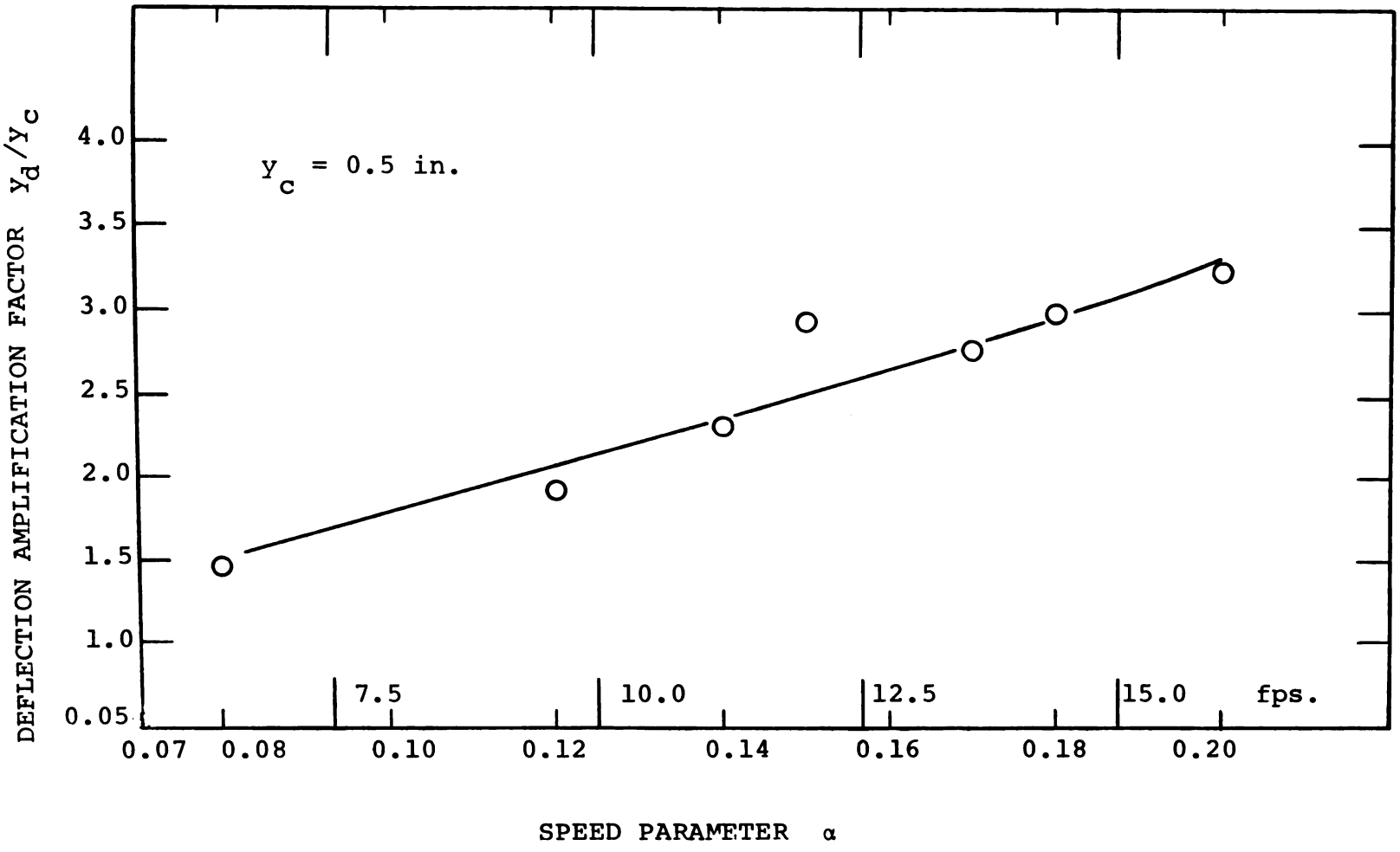

FIG. 5.3 DEFLECTION AMPLIFICATION FACTOR (β=1.3)

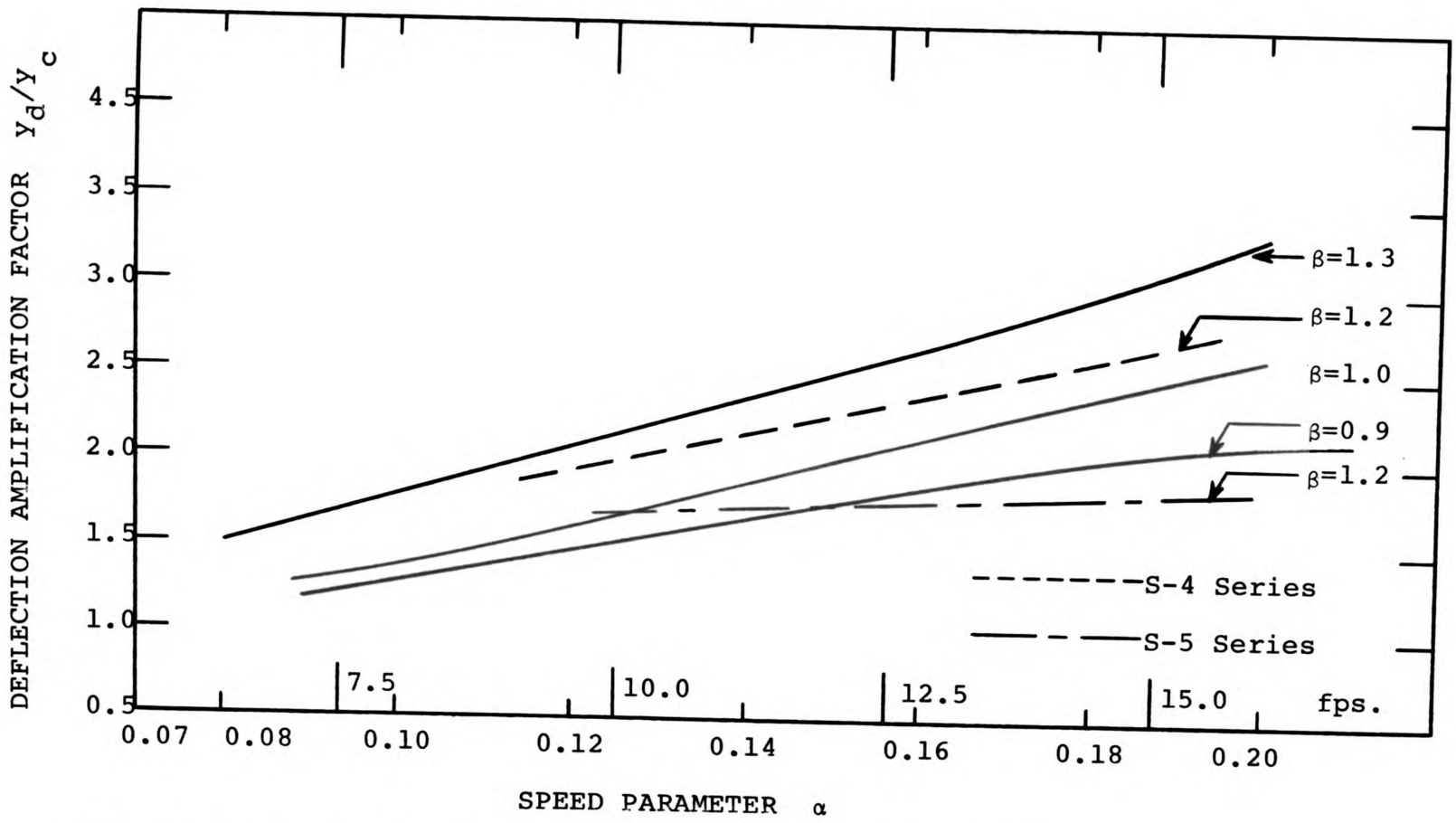

FIG. 5.4 DEFLECTION AMPLIFICATION FACTOR (FOUR β VALUES)

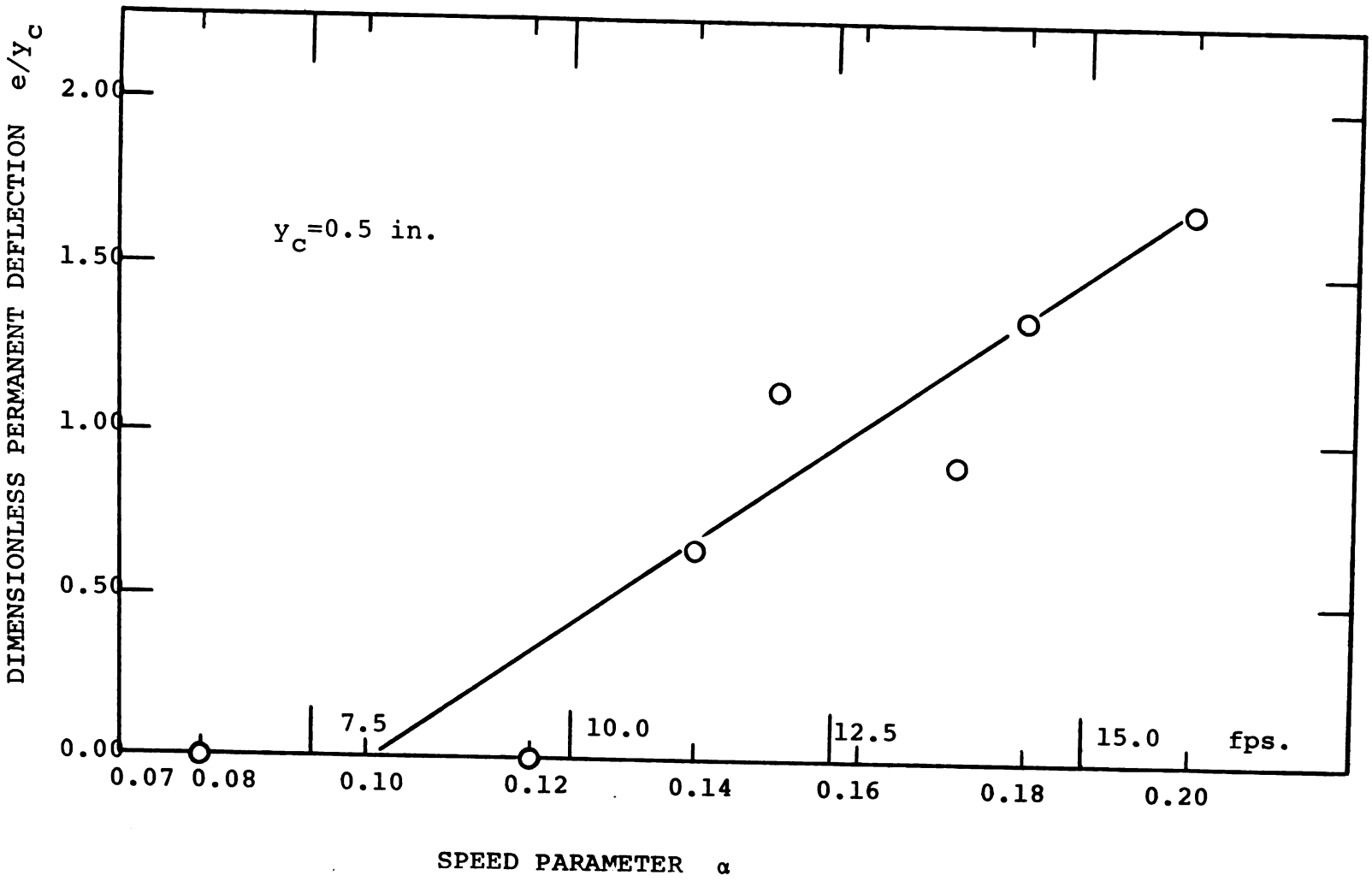

FIG. 5.5 PERMANENT DEFLECTION (β=1.3)

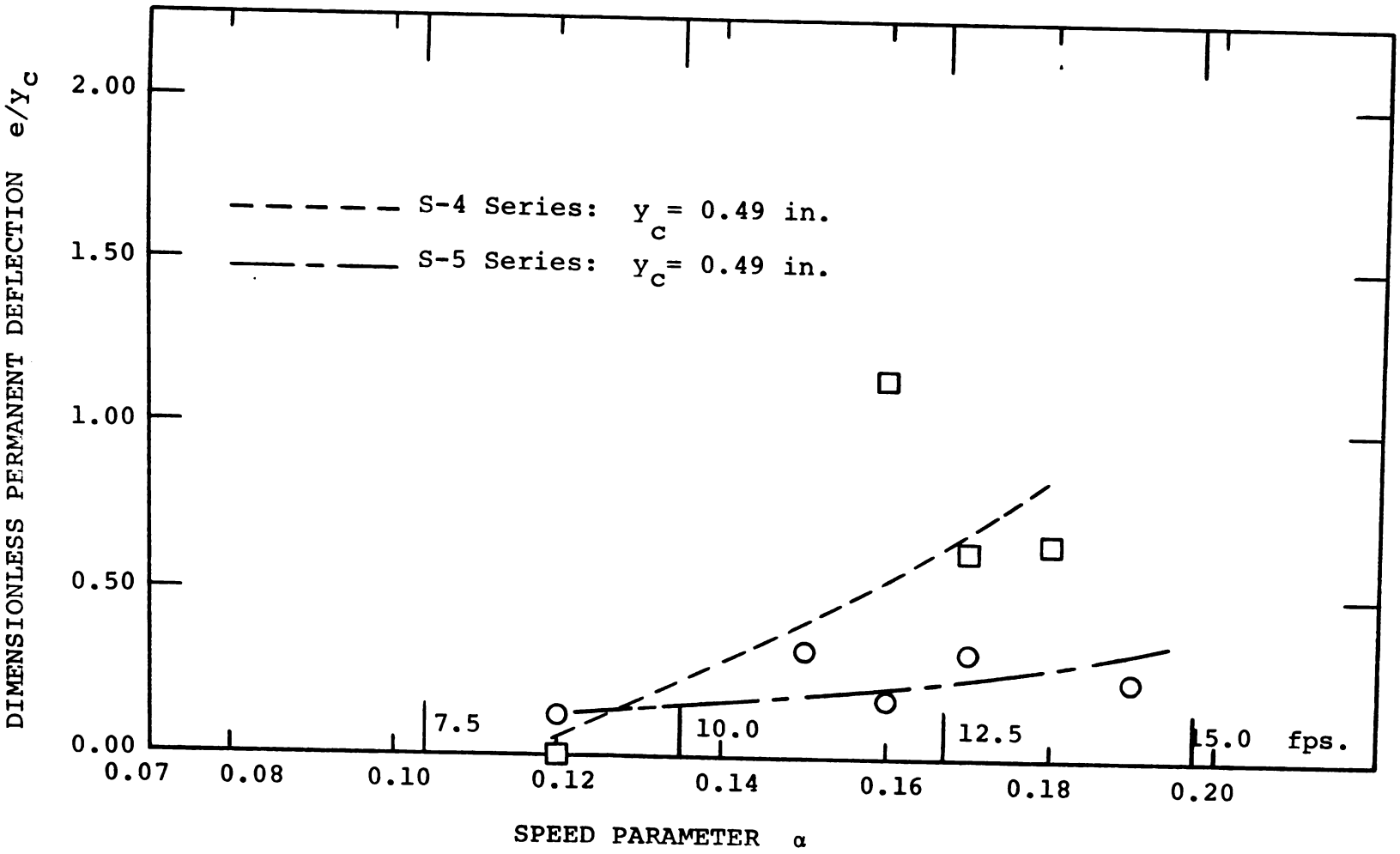

FIG. 5.6 PERMANENT DEFLECTION (β=1.2)

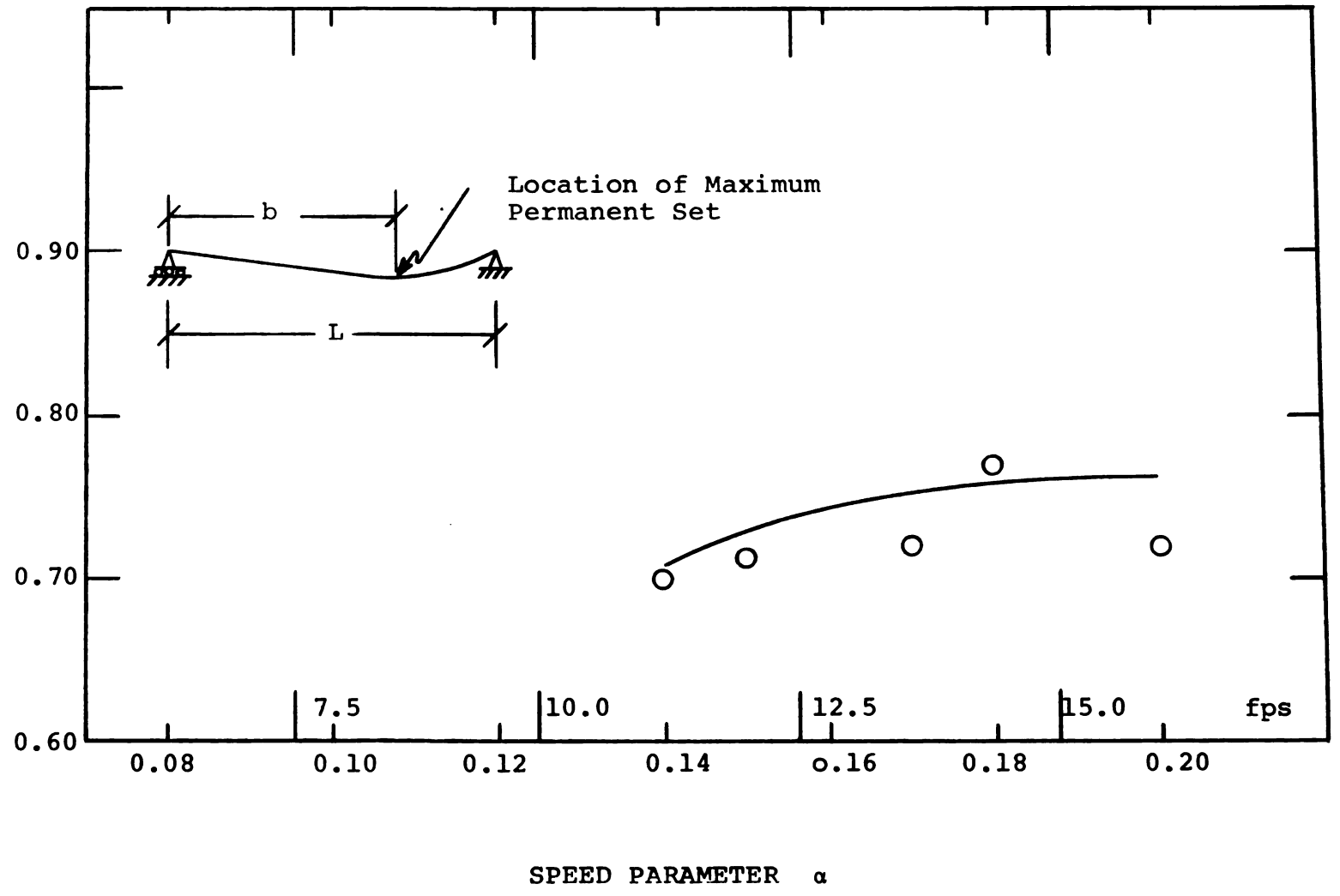

FIG. 5.7 LOCATION OF MAXIMUM PERMANENT SET (β = 1.3)

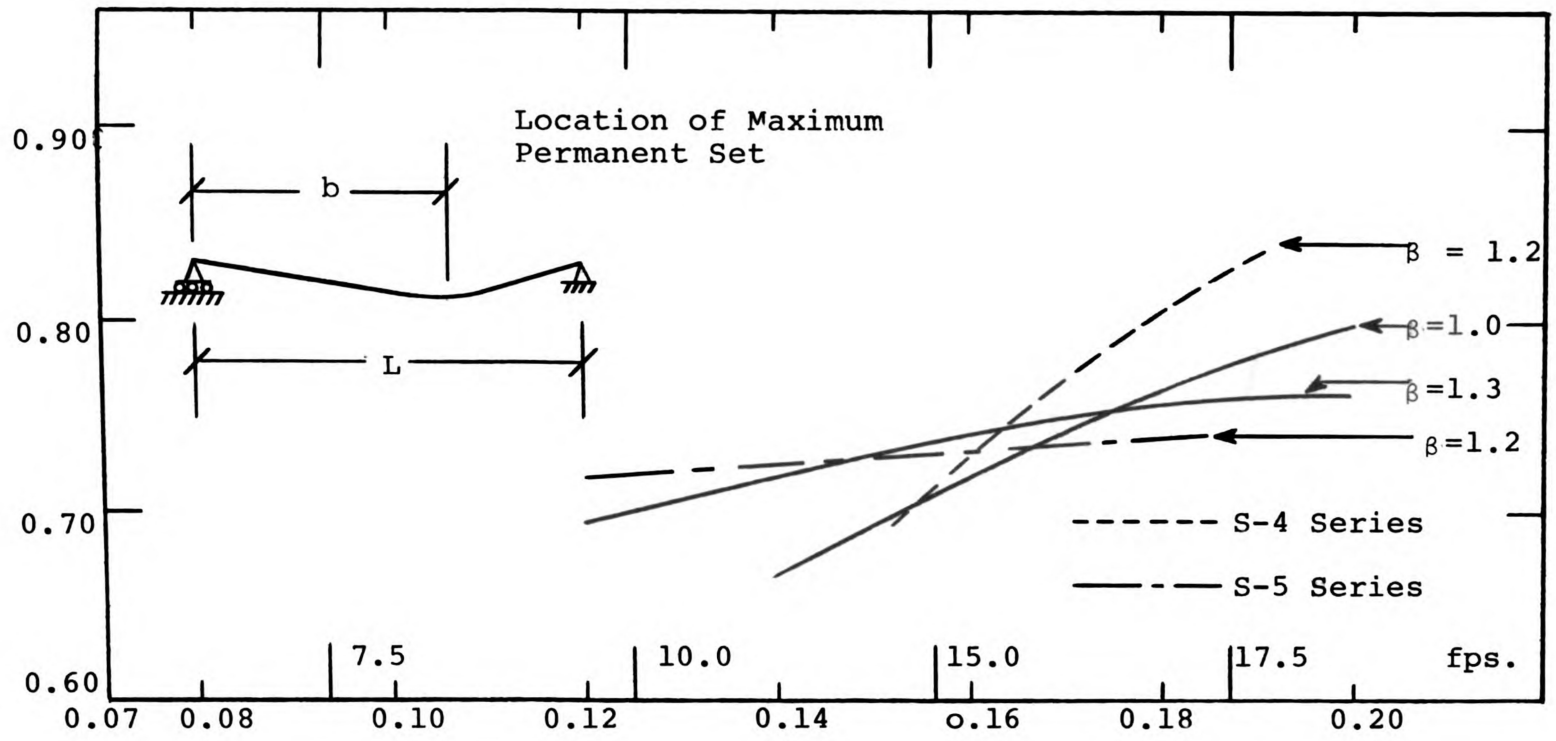

FIG. 5.8 LOCATION OF MAXIMUM PERMANENT SET (THREE β VALUES)

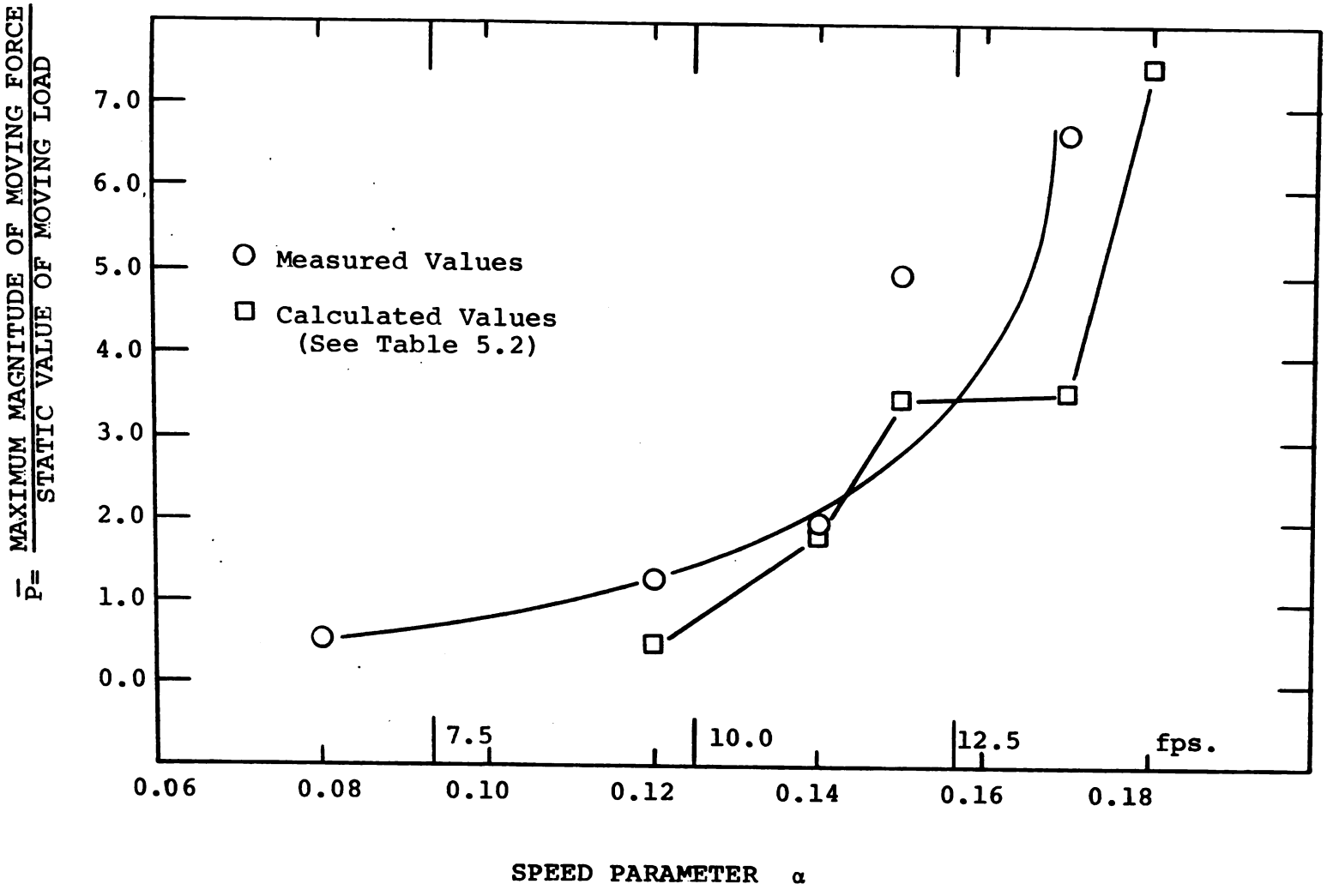

FIG. 5.9 MAXIMUM INTERACTIVE FORCE ON BEAM (β=1.3)

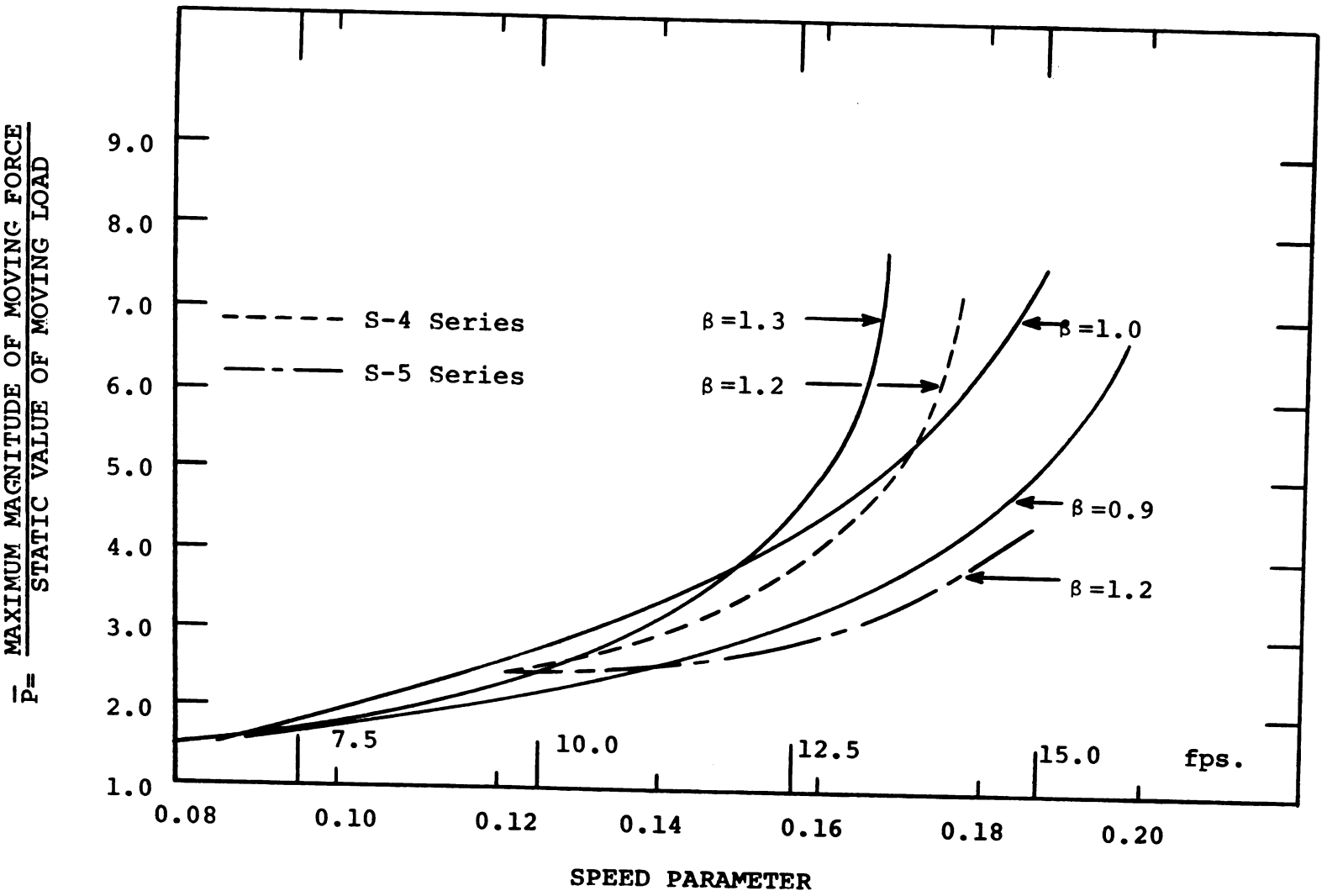

FIG. 5.10 MAXIMUM INTERACTIVF FORCE (FOUR β VALUES)

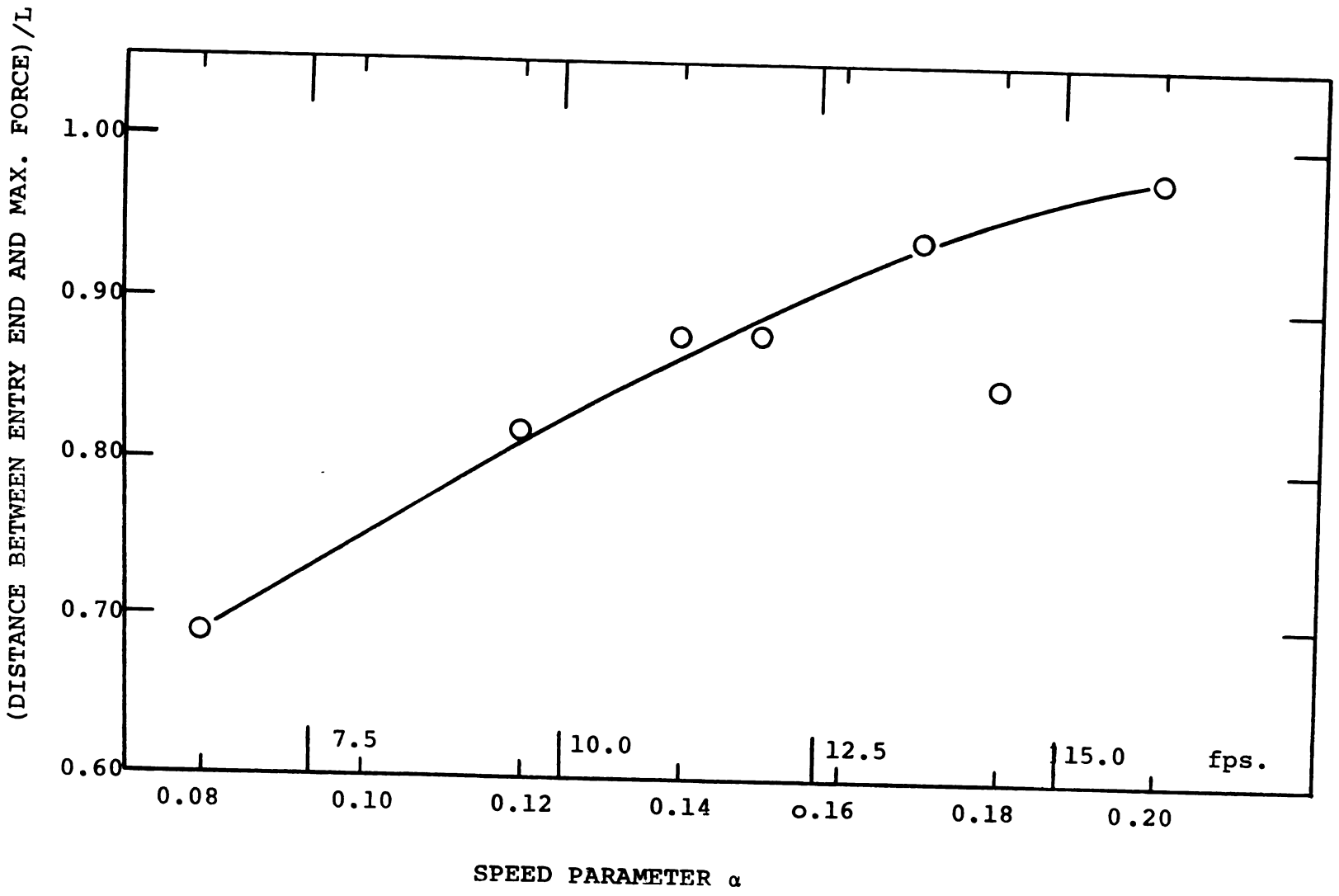

FIG. 5.11 LOCATION OF MAXIMUM FORCE (β=1.3)

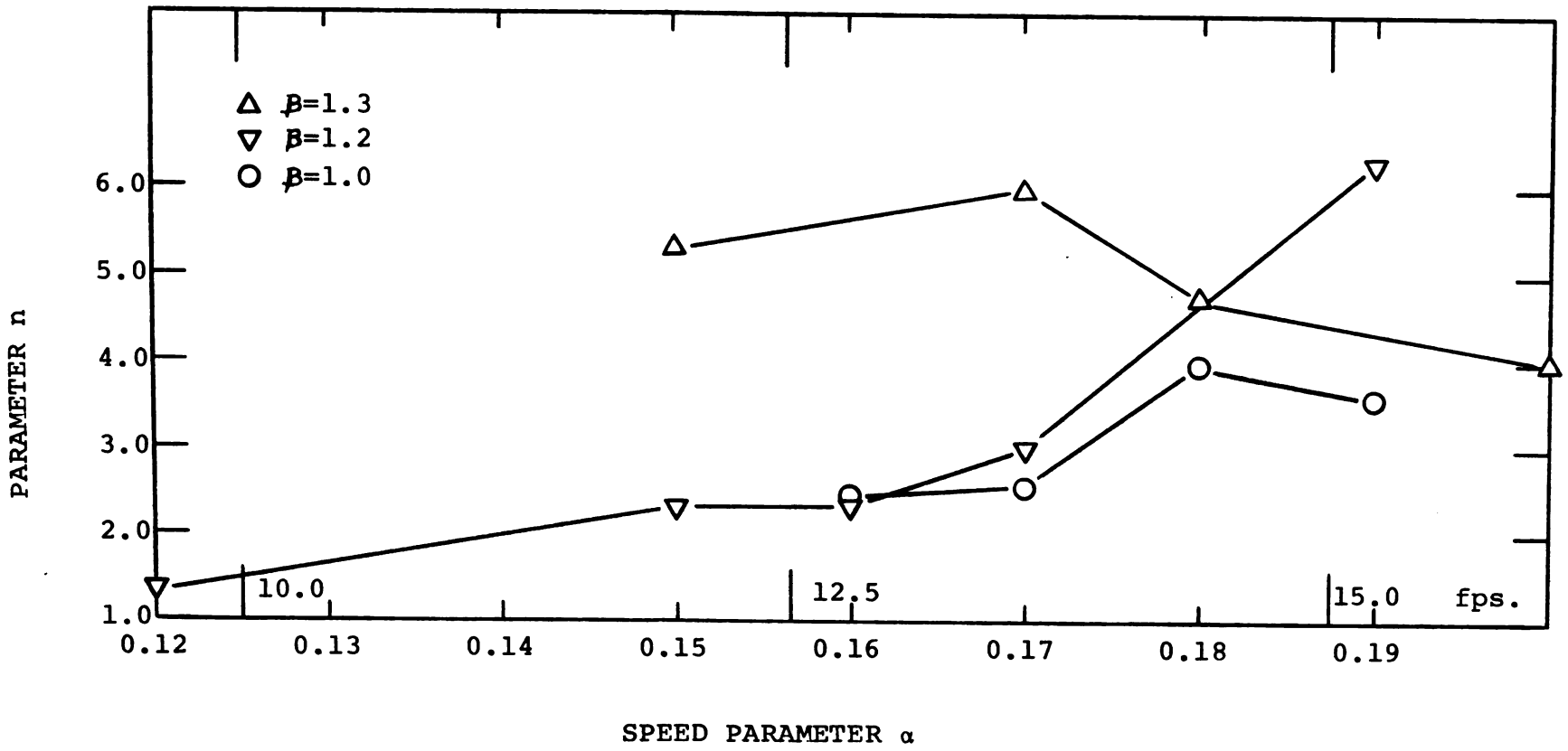

FIG. 5.12 RELATIONSHIP BETWEEN n AND α

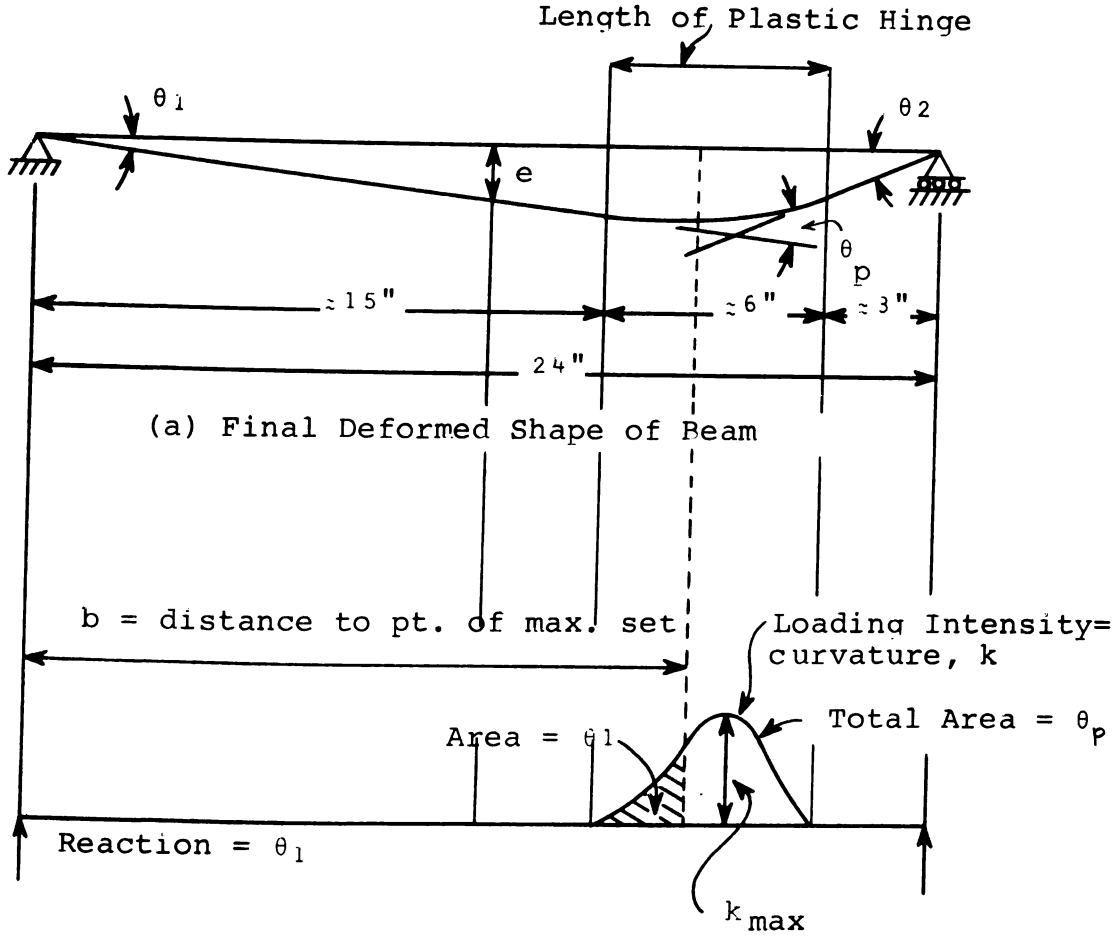

(b) "Conjugate Beam" (loaded by curvature)

FIG. 5.13 GEOMETRY OF DEFORMED BEAM

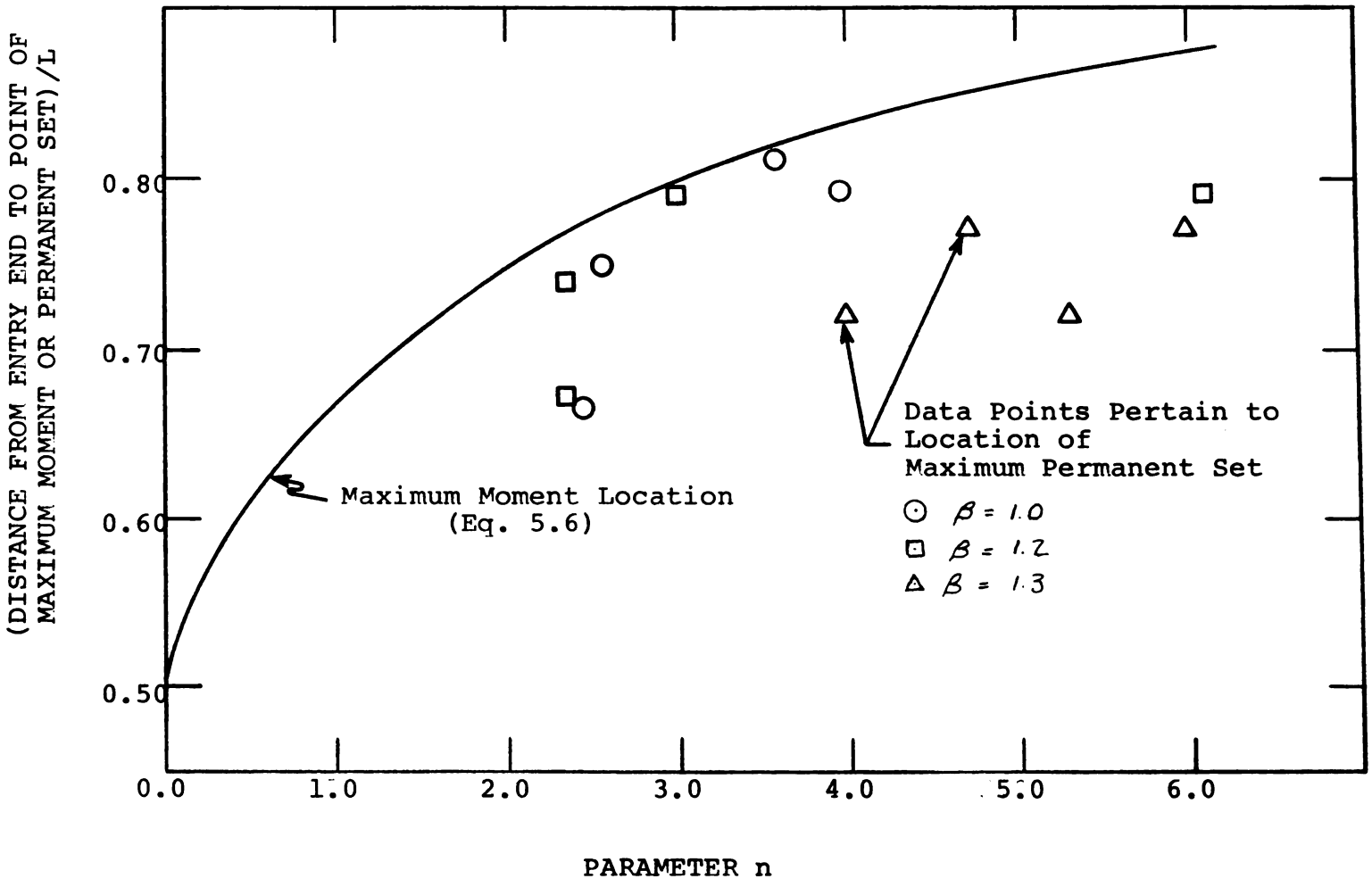

FIG. 5.14 RELATIONSHIP OF n TO POSITION OF MAXIMUM MOMENT AND TO POSITION OF MAXIMUM PERMANENT SET

Fig. 5.15 MOMENT CURVATURE RELATIONSHIP

Table 3.1 -- Yield Stress (Direct Tension in Psi)

Series	Number of Specimens	Maximum	Minimum	Mean	Standard Deviation	Coefficient of Variation %
S - 2	9	31240	29920	30300	393	1.30
S - 3	9	32200	30800	31400	454	1.44
S - 4	9	31680	30040	31100	585	1.88
S - 5	9	31680	27960	29440	909	3.08
S - 6	11	31560	28920	29700	683	2.30
S - 13	8	33680	31640	32600	579	1.78
S - 14	8	29600	28040	28670	466	1.63

Table 3.2 -- Static Moment Carrying Capacity (in-lb)

Test Number	*M_f	**M_y	$M_u = 1.5\ M_y$
S-2-2	470	325	488
S-2-8	448	316	474
S-3-2	448	320	480
S-3-8	448	321	482
S-4-2	468	329	494
S-4-8	468	331	497
S-1-4	435		
S-1-6	415		

* Beam failed in static beam test.

** $M_y = \sigma_y I/c$; σ_y from tension test.

Table 5.1 -- Data for Midspan Deflection and Maximum Permanent Set.

Test Number	α	y_d/y_c	e/y_c	b/L
		$\beta = 0.9$		
S-6-9,2	0.09	1.1	0.0	—
S-15-4,3	0.10	1.3	0.0	—
S-5-1,2	0.13	1.7	0.0	—
S-15-4,4	0.13	1.6	0.0	—
S-6-9,3	0.13	1.6	0.0	—
S-15-4,2	0.16	1.7	0.0	—
S-15-7,1	0.16	1.9	0.0	—
S-15-4,5	0.17	1.8	0.0	—
S-15-6,1	0.17	1.9	0.0	—
S-15-4,6	0.18	1.9	0.0	—
S-15-1,10	0.19	2.3	0.0	—
S-15-5,1	0.19	2.0	0.0	—
S-4-6,3	0.21	2.1	0.0	—
S-4-5,3	0.21	2.1	0.0	—
		$\beta = 1.0$		
S-14-1,2	0.09	1.5	0.0	—
S-3-1,3	0.09	1.5	0.0	—
S-3-9,1	0.12	1.6	0.0	—
S-14-1,4	0.13	1.8	0.0	—
S-3-3,1	0.14	2.0	0.0+	0.7
S-14-7,1	0.15	1.9	0.0+	—
S-14-1,5	0.16	2.1	0.1	0.7

Table 5.1 (Cont'd)

Test Number	α	y_d/y_c	e/y_c	b/L
		$\beta = 1.0$		
S-3-4,1	0.16	2.2	0.0+	0.7
S-14-3,1	0.17	1.9	0.3	—
S-3-5,1	0.17	2.3	0.0+	0.8
S-14-4,1	0.18	2.1	0.2	0.8
S-14-5,1	0.19	2.1	0.5	0.8
S-3-6,1	0.19	2.8	0.0+	0.8
S-3-7,1	0.20	2.6	0.0+	0.8
		$\beta = 1.2$		
S-5-4,1	0.12	1.7	0.1	—
S-4-3A	0.12	1.9	0.1	0.7
S-5-5,1	0.15	1.8	0.3	0.7
S-5-3,1	0.16	1.8	0.3	0.7
S-4-4A	0.16	3.0	1.1	0.7
S-5-6,1	0.17	1.8	0.3	0.8
S-4-7A	0.17	2.4	0.6	0.7
S-4-9A	0.18	2.5	0.6	0.8
S-5-7,1	0.19	1.9	0.2	0.8
		$\beta = 1.3$		
S-2-7,1	0.08	1.5	0.0	—
S-2-7,4	0.12	1.9	0.0	—
S-2-1,1	0.14	2.3	0.6	0.7
S-2-3,1	0.15	3.0	1.1	0.7
S-2-5,1	0.17	2.8	0.9	0.8

Table 5.1 (Cont'd)

Test Number	α	y_d/y_c	e/y_c	b/L
		$\beta = 1.3$		
S-2-9,1	0.18	3.0	1.4	0.8
S-2-6,1	0.20	3.3	1.7	0.7

Table 5.2 -- Maximum Moments, Curvatures and Centripedal Accelerations

1	2	3	4	5	6	7	8	9	10
Test No.	v fps.	ϕ_p $\times 10^2$	$(k_p)_a$ $\times 10^2$ in.	$(k_p)_{max}$ $\times 10^2$ in.	k max $= (k_p)_{max} + k_e$ $\times 10^2$ in.	$\frac{k\ max}{k_y}$	$\frac{(v^2 k_{max}}{g} + g)$	Maximum Moment at d in.lbs.	Max. Mom. / Static Capac.*
S-2-7	9.3	2.0	0.33	0.66	1.54	1.77	1.50		
S-2-1	11.3	8.9	1.49	2.98	3.86	4.43	2.84	612	1.30
S-2-3	12.1	16.4	2.74	5.48	6.36	7.31	4.49	618	1.31
S-2-5	13.3	13.7	2.29	4.58	5.46	6.27	4.60	576	1.22
S-2-9	14.5	25.7	4.29	8.58	9.46	10.87	8.46	673	1.43
S-2-6	15.6	31.8	5.30	10.60	11.48	13.19	11.46	731	1.55

*Static Capacity taken to be 470 in. lbs.